

UPCommons

Portal del coneixement obert de la UPC

<http://upcommons.upc.edu/e-prints>

Aquesta és una còpia de la versió *author's final draft* d'un article publicat a la revista [*Physical Review E - Statistical, Nonlinear, and Soft Matter Physics*].

URL d'aquest document a UPCommons E-prints: <http://hdl.handle.net/2117/85097>

Paper publicar¹ / Published paper:

Robles-Hernández, B., Sebastián, N., De La Fuente, MR., López, D., Díez-Berart, S., Salud, J., Ros, MB., Dunmur, D., Luckhurst, G. and Timimi, Bakir A. (2015) Twist, tilt, and orientational order at the nematic to twist-bend nematic phase transition of 1,9-bis(4-cyanobiphenyl-4-yl) nonane: A dielectric, H 2 NMR, and calorimetric study *Physical Review E - Statistical, Nonlinear, and Soft Matter Physics*, 92. 6. 062505. DOI 10.1103/PhysRevE.92.062505

¹ Substituir per la citació bibliogràfica corresponent

Twist, tilt, and orientational order at the nematic to twist-bend nematic phase transition of 1'',9''-bis(4-cyanobiphenyl-4'-yl) nonane: A dielectric, ²H NMR, and calorimetric study

Beatriz Robles-Hernández,¹ Nerea Sebastián,^{1,2} M. Rosario de la Fuente,^{1,*} David O. López,³ Sergio Diez-Berart,³ Josep Salud,³ M. Blanca Ros,⁴ David A. Dunmur,^{5,†} Geoffrey R. Luckhurst,⁵ and Bakir A. Timimi⁵

¹Departamento de Física Aplicada II, Facultad de Ciencia y Tecnología, Universidad del País Vasco, Apartado 644, E-48080 Bilbao, Spain

²Otto-von-Guericke Universität Magdeburg, Institute for Experimental Physics, ANP, 39106 Magdeburg, Germany

³Grup de Propietats Físiques dels Materials (GRPFM), Departament de Física i Enginyeria Nuclear, E.T.S.E.I.B. Universitat Politècnica de Catalunya, Diagonal 647, E- 08028 Barcelona, Spain

⁴Departamento de Química Orgánica, Facultad de Ciencias-Instituto de Ciencia de Materiales de Aragón, Universidad de Zaragoza-CSIC, E-50009 Zaragoza, Spain

⁵Chemistry, University of Southampton, Highfield, Southampton SO17 1BJ, United Kingdom

(Received 6 October 2015; published xxxxxx)

The nature of the nematic-nematic phase transition in the liquid crystal dimer 1'',9''-bis(4-cyanobiphenyl-4'-yl) nonane (CB9CB) has been investigated using techniques of calorimetry, dynamic dielectric response measurements, and ²H NMR spectroscopy. The experimental results for CB9CB show that, like the shorter homologue CB7CB, the studied material exhibits a normal nematic phase, which on cooling undergoes a transition to the twist-bend nematic phase (N_{TB}), a uniaxial nematic phase, promoted by the average bent molecular shape, in which the director tilts and precesses describing a conical helix. Modulated differential scanning calorimetry has been used to analyze the nature of the N_{TB} - N phase transition, which is found to be weakly first order, but close to tricritical. Additionally broadband dielectric spectroscopy and ²H magnetic resonance studies have revealed information on the structural characteristics of the recently discovered twist-bend nematic phase. Analysis of the dynamic dielectric response in both nematic phases has provided an estimate of the conical angle of the helical structure for the N_{TB} phase. Capacitance measurements of the electric-field realignment of the director in initially planar aligned cells have yielded values for the splay and bend elastic constants in the high temperature nematic phase. The bend elastic constant is small and decreases with decreasing temperature as the twist-bend phase is approached. This behavior is expected theoretically and has been observed in materials that form the twist-bend nematic phase. ²H NMR measurements characterize the chiral helical twist identified in the twist-bend nematic phase and also allow the determination of the temperature dependence of the conical angle and the orientational order parameter with respect to the director.

DOI: [10.1103/PhysRevE.00.002500](https://doi.org/10.1103/PhysRevE.00.002500)

PACS number(s): 61.30.Eb, 64.70.mj

I. INTRODUCTION

During the last few years interest in liquid crystal dimers has experienced an extraordinary growth due to the observation of nematic-nematic transitions for relatively simple materials where two mesogenic units are linked by methylene chains having odd numbers of carbon atoms [1–5]. Although the high temperature nematic mesophase of these materials is a conventional nematic phase, its elastic and dielectric properties are far from typical [2,6–8]. In contrast to normal low molecular weight nematic liquid crystals, odd dimers possess a bend elastic constant (K_3) significantly smaller than the splay elastic constant (K_1) [6,9,10]. Moreover, K_3 reduces with decreasing temperature reaching remarkably low values [7,9,10]. Such behavior has been successfully explained in terms of the effect the molecular shape exerts on elastic constants [11], the preferred averaged bent molecular shape promoted by the odd spacers being responsible for the low or possibly negative bend elastic constants [12]. This is especially the case when the spacer is linked by methylene groups to the mesogenic groups [13]. According to Dozov's predictions [12], a negative bend elastic coefficient [14] would give rise

to a nematic ground state where the director, instead of being uniformly aligned, spontaneously bends. This state of bend deformation would have to be accompanied by a splay or twist deformation in order to be stabilized. In the latter case, the induced twist could be left- or right-handed, and thus, even though molecules are achiral, the sample would be expected to form a conglomerate of domains having opposite chirality, that is, a nematic phase where the directors arrange themselves into a helix with the director making a constant angle with respect to it [12]. Recently we have reported [15] a twist-bend nematic (N_{TB}) mesophase for ether-linked dimers formed at low temperatures from the nematic-isotropic transition: Other authors have also claimed to have observed the twist-bend nematic phase with ether-linked dimers, but no results to support this claim are given in their paper [16].

Following a detailed investigation of the liquid crystal dimer 1'',7''-bis(4-cyanobiphenyl-4'-yl) heptane (CB7CB) [2] it was proposed that the low temperature nematic phase observed for such odd dimers is indeed the N_{TB} phase predicted by Dozov [12]. This study has been followed by intense research activity focused on the structure and properties of the N_{TB} phase. Different authors have described a characteristic ropelike texture with stripes parallel to the alignment axis for thin films of planar aligned samples [1,2,9,16,17]. With the sample between a cover slip and microscope slide, focal-conic-defect and parabolic-defect textures have been

*rosario.delafuente@ehu.es

†d.dunmur@tiscali.co.uk

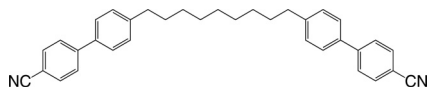


FIG. 1. Chemical structure of the methylene-linked dimer 1'',9''-bis(4-cyanobiphenyl-4'-yl) nonane (CB9CB).

of the N - I and N_{TB} - N phase transitions. Finally, our study reveals the existence of a glassy state linked to the twist-bend nematic phase.

The layout of the paper is as follows. In Sec. II we describe the experimental details. In Sec. III we present and discuss our results concerning the heat capacity data, optical microscopy, dielectric permittivity, splay and bend elastic constants, and the quadrupolar splittings from ^2H NMR spectroscopy. Our concluding remarks are summarized in Sec. IV.

II. EXPERIMENTAL DETAILS

A. Material

The symmetric liquid crystal dimer CB9CB was synthesized using the methodology previously reported for CB7CB [13]. The liquid crystalline behavior was characterized using its optical textures and modulated differential scanning calorimetry (MDSC). The phase sequence obtained (as detailed in Sec. III A) is in good agreement with earlier studies that noted a nematic-nematic phase transition in CB9CB [4], but did not identify the low-temperature phase or give any indications of its structure. Recently, Hoffmann *et al.* [27] have used ^2H NMR to study CB9CB and found that the deuterium quadrupolar tensor in the twist-bend nematic phase was uniaxial which is in accord with the global symmetry of the phase. Their results are consistent with earlier measurements made on CB7CB- d_4 [2]. Hoffmann *et al.* [27] argue that the lack of local biaxiality shows that the phase does not have the structure proposed for the twist-bend nematic. However, it has been pointed out [28] that sufficiently rapid translational diffusion along the helix axis will average out the local biaxiality, as happens with conventional chiral nematic phases. Proton NMR measurements have indeed shown that translational diffusion parallel to the helix axis is fast enough to remove the biaxiality of the quadrupolar tensor, which as a result appears to be uniaxial [28].

The ^2H NMR studies were performed on a sample of the dimer CB9CB doped with 2 wt% of CB7CB- d_4 [2]. This particular spin probe was chosen as the deuterium source because of its structural similarity to the host, CB9CB; the transition temperatures of CB7CB are just a few degrees lower than those of CB9CB; as a result the transition temperatures of the doped samples are depressed by about 1 K by the addition of the probe.

B. Experimental techniques

Heat capacity measurements at atmospheric pressure were made using a commercial differential scanning calorimeter DSC-Q2000 from TA Instruments working in the modulated mode (MDSC). Like an alternating current (ac) calorimeter, the MDSC technique, besides providing heat capacity data, simultaneously gives phase shift data that allow the determination of the two-phase coexistence region for weakly first-order phase transitions. In our work, experimental conditions were adjusted in such a way that the imaginary part of the complex heat capacity data vanished. The MDSC technique is also suitable for quantitative measurements of latent heats for first-order transitions, even if they are weak. A more detailed description of the MDSC technique can be found elsewhere [29].

79 observed [2,16], both indicative of a periodic modulation of
80 the refractive indices. However, the possibility of smecticlike
81 order was initially excluded by careful x-ray experiments,
82 which showed no Bragg reflections [2,4,7,9]. This observation
83 rules out long-range translational order in the phase, but
84 does not exclude the possibility of other structural order
85 characterized by appropriate order parameters. Through ^2H
86 NMR investigations, the chiral character of this nematic
87 phase has been unambiguously confirmed in agreement with
88 Dozov's predictions [18–21]. Recently, nanoscale helix pitch
89 periodicities of 8–10 nm have been measured in the N_{TB}
90 phase using freeze fracture transmission electron microscopy
91 (FFTEM), and similar values have been obtained from a
92 theoretical analysis of quadrupolar splittings measured for
93 8CB- d_2 dissolved in CB7CB [7,21,22]. Interestingly, although
94 composed of nonchiral molecules, electroclinic effects typical
95 of chiral systems have been also reported [23–25]. Broadband
96 dielectric studies of this compound [2,8] show that both
97 nematic mesophases have a very similar dielectric behavior. An
98 interesting question concerns the character of the N_{TB} - N phase
99 transition. Although some theoretical approaches [12,26] seem
100 to predict a second-order phase transition, calorimetric results
101 point to a first-order phase transition although with a strength
102 that changes with the molecular structure, such as the spacer
103 length [2,8].

104 The current paper focuses on the liquid crystal dimer
105 1'',9''-bis(4-cyanobiphenyl-4'-yl) nonane (hereafter referred to
106 as CB9CB; see Fig. 1) that belongs to the same homologous
107 series of methylene-linked cyanobiphenyl-alkane dimers as
108 the first reported [2] example of a twist-bend nematic phase,
109 CB7CB. High-resolution adiabatic scanning calorimetry mea-
110 surements, miscibility studies, and x-ray investigations of
111 CB9CB by Tripathi *et al.* [4] have demonstrated that, similar
112 to its shorter-chain homologue CB7CB, CB9CB exhibits two
113 nematic phases. However, in that study no mention is made
114 concerning the nature of the low temperature nematic phase.
115 In this paper we present a comprehensive experimental study
116 of both nematic phases of CB9CB that allows us to identify the
117 low temperature nematic phase as a twist-bend nematic phase.
118 The static dielectric permittivity measurements presented here
119 constitute direct evidence of changes in the conformational dis-
120 tribution in the mesophases, while studies of the dynamics of
121 the dipolar groups at the N - N_{TB} transition provide clear proof
122 of the tilt of the director in the lower temperature mesophase.
123 Since it has been proposed that elastic constants contribute
124 to the stability of the N_{TB} phase [12], K_1 and K_3 have
125 been determined using Fréedericksz-transition experiments.
126 The chiral structure associated with the heliconical twist-bend
127 nematic phase is established by ^2H NMR experiments using
128 CB7CB- d_4 as a spin probe which allows a measure of the phase
129 chirality to be established, together with the orientational order
130 and the director tilt. Additionally, by means of high-resolution
131 calorimetry experiments we present a detailed description

188 The MDSC measurements were made following different
 189 procedures. For a standard study of the overall thermal
 190 behavior of the sample, heating runs at 1 K min^{-1} from room
 191 temperature up to the isotropic phase and cooling runs at
 192 several cooling rates were performed. Additionally, in order to
 193 study the nature of the $N_{\text{TB}}-N$ and $N-I$ phase transitions, high-
 194 resolution heating and cooling runs at a rate of 0.01 K min^{-1}
 195 were performed in a temperature interval of about 5 K around
 196 the transition. Modulation parameters (temperature amplitude
 197 and oscillation period) were $\pm 0.5 \text{ K}$ and 60 s in the standard
 198 mode and $\pm 0.07 \text{ K}$ and 23 s in the high-resolution mode.
 199 Sample masses (between 2 and 3 mg) were selected to ensure
 200 a uniform thin layer within the aluminum pans.

201 Static dielectric permittivity measurements at 5 kHz were
 202 performed on an Instec cell of $8 \mu\text{m}$ thickness with antiparallel
 203 planar rubbing and a pretilt of between 1° and 3° (specified by
 204 Instec). The empty cell capacity was carefully calibrated before
 205 filling, and sealed afterward to prevent bubble formation. The
 206 experiment includes an Agilent Precision LRC meter E4890A
 207 that allows for the application of ac fields from 20 Hz to
 208 2 MHz with probe voltages up to $20 \text{ V}_{\text{rms}}$. Samples were
 209 held on a hot stage (TMSG-600) with a temperature controller
 210 (TMS-93), both from Linkam. The hot stage was placed on
 211 a polarizing microscope (BH2 Olympus) equipped with a
 212 camera (Olympus C5050) for the observation and recording
 213 of optical textures. This setup was also employed for the
 214 measurement of the splay and bend elastic constants from
 215 the voltage dependence of the capacitance of the sample
 216 through the Fréedericksz transition. The electric-field strength
 217 was varied from 0.1 to $16 \text{ V}_{\text{rms}}$, with a waiting time of 30 s
 218 between the application of the field and the acquisition of
 219 the capacitance value to guarantee the achievement of the
 220 equilibrium director distribution. Details of the data analysis
 221 are given in Sec. III B 1.

222 The complex dielectric permittivity $\varepsilon^*(\omega) = \varepsilon'(\omega) -$
 223 $i\varepsilon''(\omega)$ was measured over the frequency range $10^3 - 1.8 \times$
 224 10^9 Hz by combining two impedance analyzers: HP4192A and
 225 HP4291A. High-frequency dielectric measurements require
 226 the utilization of cells with untreated metal electrodes. In our
 227 setup the cell consists of a parallel plate capacitor made of
 228 two circular gold-plated brass electrodes 5 mm in diameter
 229 separated by $50\text{-}\mu\text{m}$ -thick silica spacers. It was placed at the
 230 end of a coaxial line and a modified HP16091A coaxial test
 231 fixture was used as the sample holder and then held in a
 232 Novocontrol cryostat, which screens the system. Dielectric
 233 measurements were performed on cooling with different
 234 temperature steps being stabilized to $\pm 20 \text{ mK}$.

235 The ^2H NMR spectra were measured on a Varian Che-
 236 matics CMX Infinity spectrometer which has a magnetic
 237 field strength of 9.40 T. In the nematic phase the director
 238 is aligned parallel to the field and in the twist-bend nematic
 239 it is the helix axis that aligns parallel to the magnetic field
 240 [18]. The sample was placed in a short NMR tube 5 mm in
 241 diameter and the tube was arranged orthogonal to the magnetic
 242 field. The sample temperature is controlled by a Chemagnetics
 243 temperature controller; it is stable to $\pm 0.3 \text{ K}$ during the
 244 spectral measurements and the transition temperatures of the
 245 doped mesogen were used to calibrate the controller to about
 246 $\pm 0.5 \text{ K}$. The spectra were measured using a single pulse
 247 sequence with a pulse width of $5 \mu\text{s}$. The relaxation delay

248 between the end of the acquisition of the free induction decay,
 249 FID and the pulse was set at 0.05 s. Typically 10000 FIDs
 250 were acquired into 4096 words of computer memory with a
 251 spectral window of 250 kHz.

252 III. RESULTS AND DISCUSSION

253 A. Mesophase behavior and calorimetry

254 The phase sequence of CB9CB was studied in the past by
 255 means of high-resolution adiabatic calorimetry and conven-
 256 tional DSC [4] revealing only two mesophases. By means of
 257 x-ray investigations the high temperature phase was identified
 258 as a conventional uniaxial nematic phase, and a second
 259 unidentified nematic phase appeared at lower temperatures [4].
 260 Our studies of CB9CB show that on cooling from the isotropic
 261 phase, a nematic phase is formed at about 394 K, as can
 262 be clearly identified from the characteristic uniform nematic
 263 texture obtained in planar cells, and the Schlieren texture
 264 formed in cells with no alignment treatment. Further cooling
 265 reveals another mesophase, which propagates along the cell
 266 leading to an initial quasiuniform texture [see Fig. 2(a)] that
 267 develops systematically into a striped texture [see Fig. 2(b)].
 268 The stripes grow slowly parallel to the surface easy axis with a
 269 periodicity of the order of twice the cell thickness as reported
 270 for other twist-bend nematic forming dimers [1,17]. For slow
 271 cooling rates, the stripes are totally developed showing tilted
 272 bands across them, as in a ropelike texture, characteristic of a

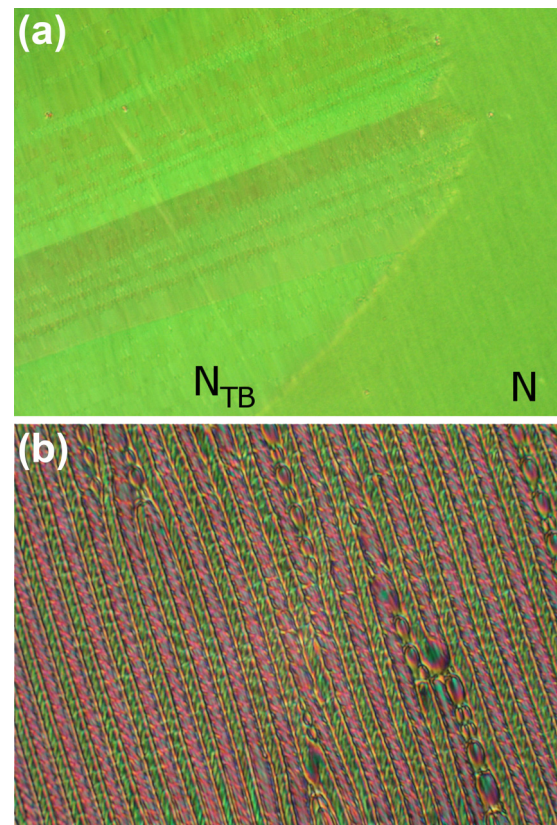


FIG. 2. (Color online) Optical textures obtained in $8\text{-}\mu\text{m}$ -thick cells (antiparallel alignment, from Instec). (a) At the $N_{\text{TB}}-N$ transition; width of the microphotograph $575 \mu\text{m}$. (b) Ropelike texture; width of the microphotograph $300 \mu\text{m}$.

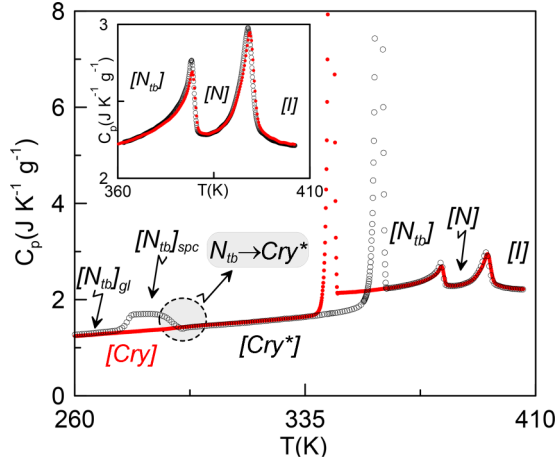


FIG. 3. (Color online) Heat capacity data as a function of temperature on heating at 1 K min^{-1} after cooling the sample from the I phase at 30 K min^{-1} (open symbols) and 1 K min^{-1} (full symbols). Inset shows a zoom on the N_{TB} - N and N - I transitions for both conditions.

twist-bend nematic phase [2], while for faster cooling rates a less uniform texture with regions of focal conics is observed. When rotating the sample with respect to the crossed polarizers bright and dark states are revealed which suggest that there are optical extinction positions that make an angle with the axis of the stripes.

Measurements of the heat capacity as a function of temperature over a wide temperature range are given in Fig. 3. Black and red symbols correspond to data recorded on heating at 1 K min^{-1} from 260 K with the sample in two different states: after cooling the sample from the isotropic phase at 30 K min^{-1} (black symbols) and after slow cooling at 1 K min^{-1} (red symbols). The fast cooling rate of 30 K min^{-1} is sufficiently high to prevent crystallization and the twist-bend nematic phase becomes a glassy state ($[N_{TB}]_{gl}$). It should be stressed that for slower cooling rates (for example, 20 K min^{-1}), the sample partially crystallizes giving rise to a coexistence of a crystalline state with a glassy state. Figure 3 clearly shows the characteristic heat capacity jump assigned to the glass transition and how the sample in the supercooled N_{TB} phase crystallizes irreversibly on heating at about 285 K (black symbols). The crystalline state obtained in this way has the same heat capacity value as the crystalline state obtained by slow cooling (red symbols) but both crystalline states are clearly different as can be inferred from the separation

of about 15 K of their melting points. Irrespective of the initial crystalline state, once the phase transition to the lower temperature nematic phase takes place, both the N_{TB} - N and the N - I phase transitions are observed to be identical as is shown in the inset of Fig. 3. The characteristic temperatures corresponding to the different phase transitions are listed in Table I.

The MDSC technique through the heat capacity data allows us to obtain the latent heat associated with the first-order phase transitions. The total enthalpy change associated with any transition (ΔH^{TOT}) can be written as

$$\Delta H^{\text{TOT}} = \Delta H + \int \Delta C_p dT, \quad (1)$$

where the second term on the right-hand side of Eq. (1) is the pretransitional fluctuation contribution (ΔC_p being the difference $C_p - C_{p,\text{background}}$ due to the change in the orientational order intrinsic to this transition) and ΔH is the latent heat which vanishes for second-order transitions. In strongly first-order phase transitions, the second term of the right-hand side of Eq. (1) can be neglected and the total enthalpy change is identified with the latent heat associated with the phase transition. This applies to the latent heat obtained for the $\text{Cry}-N_{TB}$ transition (considering the crystal phase formed by slow cooling), and the result is listed in Table I. The results are in quite good agreement with the value reported by Tripathi *et al.* [4]. The latent heat associated with the N - I and N_{TB} - N phase transitions deserves a special mention and will be analyzed in the following sections: Secs. III A 1 and III A 2.

1. The N - I phase transition

The theoretical description of the uniaxial N - I phase transition through the Landau-de Gennes theory is similar to the mean-field Landau model, but in the free energy density expansion of the nematic phase in terms of the scalar order parameter Q_N , identified with the average value of the second Legendre polynomial $\langle P_2(\cos \theta_i) \rangle$ with θ_i the angle of the i th molecule with respect to the nematic director, a cubic term B is needed:

$$F_N = F_I + A Q_N^2 + B Q_N^3 + C Q_N^4 + D Q_N^6 + \dots \quad (2)$$

The B parameter is the so-called cubic invariant and is responsible for the first-order character of the N - I phase transition. If B is very small and the other parameters A and C become simultaneously zero, the N - I phase transition

TABLE I. Transition temperatures ($T_{\text{Cry}N_{TB}}$, T_g , $T_{N_{TB}N}$, and T_{NI}) and transition entropies ($\Delta S_{\text{Cry}N_{TB}}/R$, $\Delta S_{N_{TB}N}/R$, and $\Delta S_{NI}/R$).

$T_{\text{Cry}N_{TB}}$ (K)	$\Delta S_{\text{Cry}N_{TB}}/R$	T_g (K)	$T_{N_{TB}N}$ (K)	$\Delta S_{N_{TB}N}/R$	T_{NI} (K)	$\Delta S_{NI}/R$	Reference
–	–	–	377.22	0.037 ± 0.002	392.92	0.18 ± 0.02	Ref. [4] ^a
			380.45	–	395.90	–	Ref. [4] ^b
357.6 ^c	10.6 ^c	277.2 ^d	379.09	0.038 ± 0.006^e	394.92	0.16 ± 0.02^e	This work

^aData from adiabatic scanning calorimetry (ASC) at 0.15 K h^{-1} .

^bData from DSC traces.

^cFrom MDSC data on heating at 1 K min^{-1} . The sample was previously cooled at 1 K min^{-1} .

^dFrom MDSC data on heating at 1 K min^{-1} . The sample was previously cooled at 20 K min^{-1} .

^eFrom MDSC data on heating at 0.01 K min^{-1} .

338 becomes strictly tricritical [30,31]. In such a situation the heat
 339 capacity critical exponent α in both the N and I phases must
 340 be $\frac{1}{2}$ and the Q_N critical exponent β must be $\frac{1}{4}$. From an
 341 experimental point of view, such parameters can be obtained
 342 from very accurate heat capacity data through the N - I phase
 343 transition.

344 Figure 4 shows the heat capacity together with the ϕ -phase
 345 shift data around the N - I phase transition. The sharp peak in

$$C_{p,I} = B_C + D_C \left[\frac{T}{T^*} - 1 \right] + A_{C,I} \left| \frac{T}{T^*} - 1 \right|^{-\alpha}, \quad \text{for } T > T_{NI} = T^* + \Delta T^*, \quad (3a)$$

$$C_{p,N} = B_C + D_C \left[\frac{T}{T^{**}} - 1 \right] + A_{C,N} \left| \frac{T}{T^{**}} - 1 \right|^{-\alpha}, \quad \text{for } T < T_{NI} = T^{**} - \Delta T^{**}. \quad (3b)$$

354 The exponent α (the same in the N and I phases), both
 355 spinodal temperatures T^{**} and T^* , the B_C and D_C terms
 356 corresponding to the so-called heat capacity background, and
 357 the corresponding amplitudes $A_{C,N}$ and $A_{C,I}$ are found by
 358 fitting the experimental data of Fig. 4 to Eqs. (3a) and (3b).
 359 In the methodology followed, the common parameters in both
 360 phases (B_C , D_C , and α) have been simultaneously refined after
 361 a previous independent fitting. The most significant parameters
 362 ($A_{C,N}/A_{C,I}$, T^* , T^{**} , and α) that characterize the nature of the
 363 N - I phase transition are listed in Table II. All of the fitted
 364 parameters represent well the measured heat capacity data as
 365 is seen in Fig. 4 where both Eqs. (3a) and (3b) are drawn.

366 The latent heat associated with the N - I phase transition is
 367 calculated using Eq. (1) from the heat capacity data of Fig. 4.
 368 Our value is listed in Table I and is in quite good agreement
 369 with the value reported by Tripathi *et al.* [4].

370 The critical behavior of the scalar order parameter Q_N
 371 around the N - I phase transition as a function of temperature
 372 has been studied by calculating $Q'_N = (a_0/2T^*\rho_N)^{1/2} Q_N$,
 373 according to the methodology first used by others [34] and
 374 successfully applied by us elsewhere [32,33,35]. The scalar

346 ϕ -phase shift data at the transition temperature is a signature
 347 of the first-order character of the N - I phase transition and will
 348 be used to delimit the coexistence region by the dashed lines
 349 in Fig. 4.

350 The critical behavior of the heat capacity around the
 351 N - I phase transition follows the standard expressions
 352 [15,30,32,33] in a region of no more than ± 3 K around
 353 T_{NI} :

375 order parameter $Q_N(T)$ can be written as

$$Q_N^2(T) = \frac{2\rho_N T^*}{a_0} \left[\int_{T_I}^{T_{CI}} \frac{\Delta C_p}{T} dT + \frac{\Delta H_{NI}}{T_{NI}} + \int_{T_{CN}}^T \frac{\Delta C_p}{T} dT \right], \quad (4)$$

376 where ρ_N is the density of the liquid crystal in the nematic
 377 phases and the constant a_0 is the first coefficient in the Landau-
 378 de Gennes expansion [$A = a_0(T - T_0)/T_0$]. The integration
 379 of Eq. (4) has been made numerically on cooling from T_I in
 380 the isotropic phase, well above T_{NI} , at which Q_N could be
 381 considered zero down to T . Both temperatures, T_{CI} and T_{CN} ,
 382 are the limiting temperatures of the coexistence region in the
 383 isotropic and nematic phases, respectively. The terms ΔH_{NI}
 384 and ΔC_p are the latent heat and the difference between the
 385 heat capacity and the heat capacity background, respectively.
 386 The Landau-de Gennes theory provides the generic expression
 387 [30]

$$Q'_N = Q'_N{}^{**} + K|T - T^{**}|^\beta, \quad \text{for } T < T^{**} - \Delta T^*. \quad (5)$$

388 The inset of Fig. 4 shows how well our calculated Q'_N data
 389 are fitted by Eq. (5) with a β critical exponent of 0.25 and
 390 the spinodal temperature T^{**} with the same value obtained
 391 through Eqs. (3a) and (3b) (see Table II).

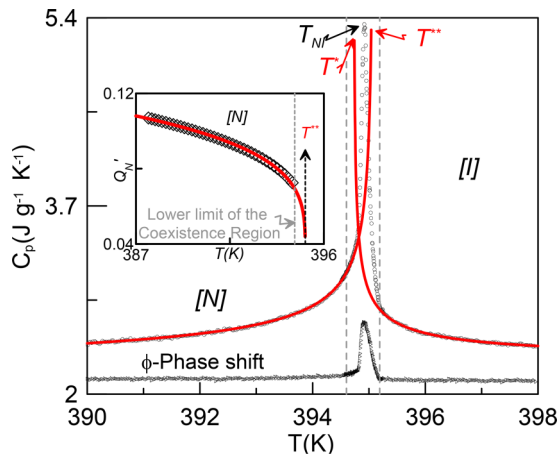


FIG. 4. (Color online) Heat capacity data as a function of tem-
 perature near the N - I phase transition. The limits of the heat capacity
 coexistence region (delimited by the vertical dashed lines) are defined
 by the phase shift angle data. Solid lines are fittings according to
 Eqs. (3a) and (3b). The inset shows Q'_N data as a function of
 temperature together with the corresponding fitting to Eq. (5).

2. The N_{TB} - N phase transition

392 Recently, some interesting models for the N_{TB} - N phase
 393 transition according to the Landau theory have been published
 394 [14,25,36]. In such models, the Oseen-Frank free energy is
 395 taken as the starting point for the modeling of a twist-bend
 396 nematic phase, but additional order parameters are required
 397 to account for the heliconical structure (tilt and twist) of the
 398 twist-bend nematic phase. Shamid *et al.* [14] propose a detailed
 399 approach based on the existence of polar order and bend
 400 coupling, i.e., a coupling which favors polar order along the
 401 bend. These theoretical approaches give rise to a second-order
 402 N_{TB} - N phase transition that, to date, has never been found.
 403 Experimental results for CB7CB, the most studied material
 404 exhibiting a twist-bend nematic-nematic phase transition,
 405 give a nonzero latent heat ($\Delta H_{N_{TB}N}$) [2] and an apparent
 406 discontinuity [37] of the conical angle, which, as in the Dozov
 407 Landau like model and molecular-field theory [26], is one of
 408 the possible order parameters characteristic of the N_{TB} phase.
 409 The latent heat ($\Delta H_{N_{TB}N}$) for the N_{TB} - N transition of CB9CB
 410

TABLE II. Parameters of the fitting of the N_{TB} - N and the N - I phase transitions.

Physical property	N_{TB} - N		N - I			
	T_1 (K)	T_0 (K)	T^{**} (K)	T^* (K)	$A_{C,N}/A_{C,I}$	α
Heat capacity	379.3 ^a	378.8 ^a	395.1 ^a	394.7 ^a	1.6 ± 0.4	0.50 ± 0.05
Order parameter	–	–	395.1 ^a	–	–	–

^aThe error in temperature is of ±0.1.

411 was measured by Tripathi *et al.* [4] using high-resolution
 412 adiabatic calorimetry. In the present study, using the MDSC
 413 technique, $\Delta H_{N_{TB}N}$ is estimated using Eq. (1) from the heat
 414 capacity data of Fig. 5, and our value, listed in Table I, is in
 415 very good agreement with this. These results clearly indicate
 416 the first-order character of the N_{TB} - N phase transition. In
 417 addition, the data in Fig. 5 show an evident similarity to the heat
 418 capacity data around the N_{TB} - N phase transition for CB7CB,
 419 reported by us some years earlier [2]. At that time, the analysis
 420 of the critical behavior in the proximity of the N_{TB} - N phase
 421 transition was made by using the well-known and very simple
 422 phenomenological mean-field Landau model.

423 A very recent theoretical study made by Kats and Lebedev
 424 [38] argues that because of the short pitch of the helicoidal
 425 structure [7,22] the description of the N_{TB} phase based on the
 426 Oseen-Frank free energy requires modification and that the
 427 polar order should not be included. The chosen order parameter
 428 is a vector φ containing the conical angle and the pitch of
 429 the helicoidal structure. Minimizing the proposed Landau
 430 functional with respect to the tilt angle and neglecting short-
 431 range fluctuations of the order parameter leads to the standard
 432 result of the mean-field Landau model. According to this study,
 433 the heat capacity of the twist-bend nematic phase close to the
 434 phase transition should be expressed as

$$C_p^{N_{TB}} = C_p^N + A^*[T_K - T]^{-1/2}, \quad (6)$$

435 where the heat capacity of the nematic phase (C_p^N) is described
 436 by the linear function

$$C_p^N = B^* + C^*[T - T_0]. \quad (7)$$

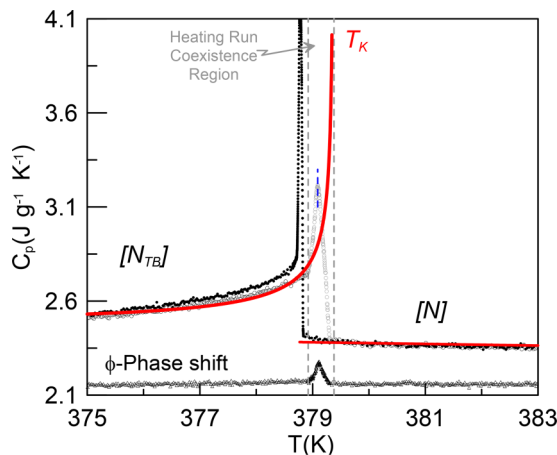


FIG. 5. (Color online) Heat capacity data as a function of temperature near the N - N_{TB} phase transition. The limits of the heat-capacity coexistence region (delimited by the vertical dashed lines) are defined by the phase shift angle data. Solid lines are fittings according to Eqs. (6) and (7).

The temperature T_K represents the temperature of the
 metastability limit for the twist-bend nematic phase on heating.
 The coefficients A^* , B^* , and C^* and the temperatures T_K
 and T_0 of both Eqs. (6) and (7) are obtained as fitting
 parameters from the experimental results of high-resolution
 heat capacity data in the vicinity of the N_{TB} - N phase transition,
 but close to the phase transition. In fact, there are two
 characteristic temperatures in the mean-field Landau model:
 The temperatures T_0 and T_1 are those at which second-order
 and first-order phase transitions take place, respectively. The
 temperature T_K is related to both T_0 and T_1 by means of the
 relationship

$$T_K = \frac{4}{3}T_1 - \frac{1}{3}T_0. \quad (8)$$

When the phase transition is considered tricritical, T_0 is set
 equal to T_1 and coincides with T_K .

Figure 5 shows the heat capacity for CB9CB in the vicinity
 of the N_{TB} - N phase transition (heating run: empty symbols;
 cooling run: full symbols) and the ϕ -phase shift data show
 a sharp peak which is a signature of the first-order character
 of the phase transition. This peak is used to determine the
 coexistence region (indicated by dashed lines in Fig. 5). Our
 heat capacity data have been fitted to Eqs. (6) and (7) and
 both equations are drawn (red lines) in Fig. 5. The two
 characteristic temperatures, T_0 and T_1 , are listed in Table II.
 The key result from our fit is the value of $T_K/T_0 = 1.0018$ and
 using Eq. (8), $T_1/T_0 = 1.0014$. Both temperature ratios are
 compatible with a first-order N_{TB} - N phase transition, but one
 which is nearly tricritical. For the shorter-chain homologue,
 CB7CB, this transition was analyzed according to the same
 theoretical model and the results are similar [2], though the
 longer spacer in CB9CB will be expected to influence the
 details of the transitional behavior. These results point to
 a first-order phase transition although with a strength that
 changes with the molecular structure, such as the spacer length
 [2,8]. Thus, for CB9CB the associated latent heat of the
 N_{TB} - N phase transition is about 125 J mol⁻¹ whereas for
 CB7CB it is about 205 J mol⁻¹.

B. Dielectric studies

In liquid crystal dimers, molecular flexibility provided by
 the spacer, and the corresponding changing distribution of
 conformers, has a major effect on the energetically favored
 molecular shapes and thus, on the mesophase properties
 [39,40]. The conformational distribution is also influenced
 by the anisotropic nematic interactions, favoring molecular
 geometries that can better adapt to the nematic ordering and
 environment. The temperature dependence of the dielectric
 response of a liquid crystal phase depends on the rotational
 distribution of the molecular dipoles in the presence of an

484 electric field and the orientational order of the phase. However,
 485 the order parameter itself is temperature dependent, and,
 486 as indicated previously, both the molecular dipoles, through
 487 the shape, and the order parameter are affected by the
 488 conformational distribution.

489 Calculations of the conformational energy as a function
 490 of the angle between the two terminal mesogenic groups
 491 have been carried out using a continuous torsional potential
 492 for the flexible chain segments. The results have shown
 493 that the CB7CB homologue has a temperature dependent
 494 conformational distribution characterized by a strong, broad
 495 peak centered around 120° (extended conformers) and a weak
 496 peak at 30° (hairpin conformers) [2]. These calculations also
 497 show that the increase of the orientational order parameter
 498 is accompanied by the growth of the proportion of extended
 499 conformers and in addition, by a slight increase of the angle
 500 between mesogenic units; i.e., the average molecular shape is
 501 adapting to the increased orientational order in the nematic
 502 environment [41].

503 Electric dipoles can be used as effective molecular probes
 504 to detect changes in molecular structure via dielectric mea-
 505 surements. Dielectric permittivity provides a measure of the
 506 averaged molecular mean-square dipole moment, which is
 507 determined by the conformationally averaged vector sum of
 508 the constituent dipoles and, hence, is directly related to the
 509 distribution of molecular conformations [15,42–44]. For the
 510 dimers CB7CB and CB9CB, the mean-square dipole moment
 511 is given by the averaged vector sum of the dipole moments
 512 associated with the nitrile groups attached to the terminal
 513 mesogenic units. The different molecular conformers will
 514 contribute differently to the measured components of the
 515 dielectric permittivity. Thus the extended conformers having
 516 an angle between the terminal dipoles of around 120° will
 517 have a zero mean-square dipole component contributing to the
 518 parallel permittivity along the director. For such conformers
 519 there will be a nonzero contribution (transverse) of the dipoles
 520 to the perpendicular component of the permittivity, which will
 521 depend on the angle between the terminal dipolar groups.
 522 Hairpin conformers will have a large mean-square dipole
 523 moment contribution to the parallel permittivity measured
 524 along the director. Furthermore, the relaxation rates for the
 525 transverse and longitudinal dipole polarizations are different,
 526 and so changes of the conformational distribution of the
 527 interarm angle should be clearly reflected by measurements
 528 of the dielectric permittivity.

529 We have performed measurements of the parallel and
 530 perpendicular static dielectric permittivity components of
 531 CB9CB on cooling from the isotropic phase. The perpendic-
 532 ular component of the permittivity (ϵ_{\perp}) was directly obtained
 533 using harmonic probe fields of low amplitude ($0.5 V_{\text{rms}}$) well
 534 below the threshold voltage of the Fréedericksz transition. On
 535 the other hand, the parallel component (ϵ_{\parallel}) was measured
 536 by applying voltages well above the transition, which aligns
 537 the director parallel to the field. Both components were
 538 measured as a function of temperature at various frequencies.
 539 Results show that capacitance measurements are significantly
 540 influenced by undesired ionic effects for frequencies below
 541 5 kHz, particularly for the parallel component, and so the
 542 static dielectric permittivity was determined at 5 kHz as shown
 543 in Fig. 6(a). This frequency is well below the characteristic

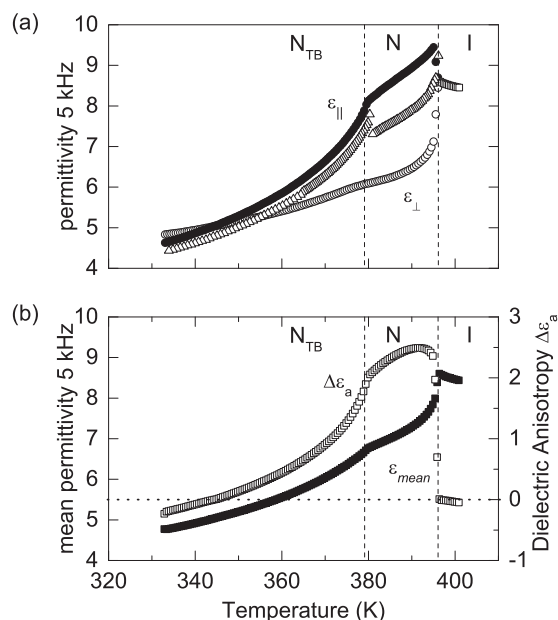


FIG. 6. (a) Temperature dependence of the static permittivity: (□) isotropic phase, (○) perpendicular component, and (•) parallel component. Open triangles (△) correspond to the parallel component of the permittivity measured with dc bias in metallic cells. (b) Temperature dependence of the (■) mean permittivity and (□) dielectric anisotropy.

544 frequency of the lowest relaxation over the whole temperature
 545 range as will be shown later. Additionally, the mean dielectric
 546 permittivity [$\bar{\epsilon} = (\epsilon_{\parallel} + 2\epsilon_{\perp})/3$] and the dielectric anisotropy
 547 ($\Delta\epsilon_a = \epsilon_{\parallel} - \epsilon_{\perp}$) are shown in Fig. 6(b) as a function of
 548 temperature. Open triangles in Fig. 6(a) represent the static
 549 dielectric permittivity obtained with metallic cells under dc
 550 bias conditions. Static dielectric permittivity measurements
 551 for CB9CB show a temperature dependence similar to that
 552 reported for other symmetric dimers [2,6,42] and clearly reflect
 553 the phase transitions detected optically and by calorimetric
 554 studies. As expected for materials with positive dielectric
 555 anisotropy, the value of the perpendicular component of the
 556 permittivity decreases on cooling from the isotropic phase
 557 while the parallel component increases at the isotropic-to-
 558 nematic transition. For odd dimers, this increase can be
 559 explained in terms of the slight stabilization of hairpin
 560 conformers at the onset of nematic ordering. However, after
 561 this initial growth the parallel permittivity starts to decrease
 562 in the nematic phase on further reducing the temperature. As
 563 can be observed in Fig. 6(b), this trend entails a progressive
 564 increase of the difference between the mean permittivity and
 565 the extrapolated isotropic value with decreasing temperature,
 566 i.e., a significant reduction of the average molecular mean-
 567 square dipole moment as the orientational order of the phase
 568 increases. As mentioned before, this fact can be explained
 569 satisfactorily by the progressive increase in the population of
 570 extended conformers with zero longitudinal dipole moment,
 571 which is driven by the increase of orientational order [41].

572 On entering the N_{TB} phase, the decrease with lowering tem-
 573 perature of both components of the permittivity is accelerated,

574 and at low temperatures there is a sign reversal in the dielectric
575 anisotropy from positive to negative.

576 1. Permittivity measurements as a function 577 of temperature and frequency

578 To gain insight into the rotational dynamics of the dipolar
579 groups, measurements of the frequency dependent dielectric
580 permittivity were made. The interpretation of the dielectric
581 absorption of dimers as a function of frequency has required
582 the development of a suitable theoretical model based on a
583 time-scale separation between the motion of the mesogenic
584 units and the fast relaxation of the flexible chain [41].
585 This model assumes that the molecular reorientation occurs
586 via the individual orientational relaxation of the mesogenic
587 units (end-over-end processes) and excludes whole molecule
588 reorientation, which would require the simultaneous reversal
589 of both terminal groups, for which the corresponding energy
590 barrier is too high. For symmetric dimers, such as CB9CB, a
591 single low-frequency absorption whose strength depends on
592 the population distribution of conformers is predicted.

593 The dynamic dielectric response of CB9CB was investi-
594 gated in 50- μm -thick metallic cells under two dc bias condi-
595 tions (0 and 35 V). As will be shown later, in measurements
596 without dc bias, metal surface interactions induce planar
597 alignment allowing us to obtain the perpendicular component
598 of the permittivity. The application of a dc bias reorients the
599 sample and the permittivity saturates at high voltages. Results
600 obtained for the static permittivities of CB9CB using both
601 the 8- μm glass Instec cell and the 50- μm metal cell are
602 shown in Fig. 6. From the comparison of the parallel static
603 permittivity components given in Fig. 6(a), it is clear that
604 the alignment obtained in 50- μm cells with dc bias is not
605 equivalent to that achieved in 8- μm cells with ac bias. Textures
606 observed when applying a dc bias in glass cells indicate that
607 the divergence between both alignments can be assigned to
608 director fluctuations caused by convective instabilities. For the
609 variable frequency measurements, it is only possible to obtain
610 values for the parallel component of the permittivity (ϵ_{\parallel}) from
611 50- μm metal cells with dc bias. The frequency dependence of
612 the real and imaginary parts of the perpendicular and parallel
613 dielectric permittivity components are given, respectively, in
614 Figs. 7 and 8 for temperatures in the nematic and twist-
615 bend nematic phases. The dielectric response of CB9CB in
616 the nematic phase, like that of its homologue CB7CB, is
617 characterized by two relaxation processes whose contribution
618 to the dielectric spectrum depends on the alignment of the
619 director in the measurement cell. These dielectric relaxations
620 can be associated with the rotational diffusion of the dimer
621 molecules: an end-over-end reorientation of the dipolar groups
622 parallel to the director at low frequencies (m_1), in agreement
623 with the theoretical model for dielectric relaxation in nematic
624 dimers [40], and the precessional motion of the dipolar groups
625 around the director for the high-frequency branch of the
626 spectrum (m_2). The frequency and temperature dependences
627 of the dielectric absorption, represented as three-dimensional
628 plots, are given for both alignments in Fig. 7(a) (perpendicular
629 to \mathbf{n}) and Fig. 8(a) (parallel to \mathbf{n}).

630 For each temperature and director alignment the frequency
631 dependence of the permittivity has been analyzed by fitting

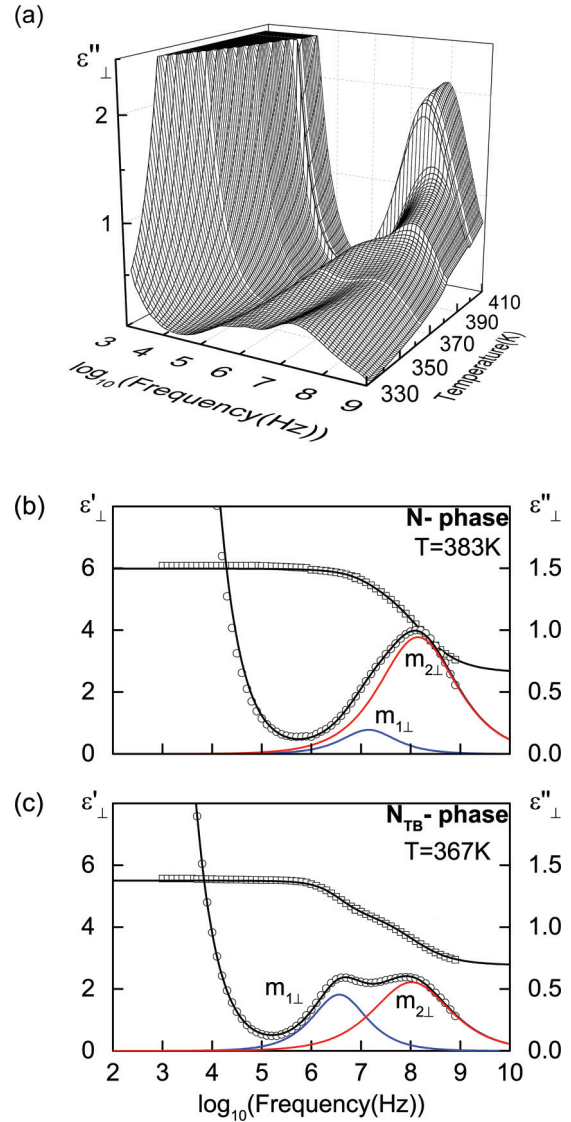


FIG. 7. (Color online) Perpendicular alignment. (a) Three-dimensional plot of the dielectric losses vs temperature and logarithm of the frequency. Frequency dependence of ϵ'_{\perp} (\square) and ϵ''_{\perp} (\circ) (b) in the N phase, and (c) in the N_{TB} phase. In (b) and (c) solid lines are fits to Eq. (9).

each relaxation mode according to the Havriliak-Negami function through the empirical relationship

$$\epsilon(\omega) - \epsilon_{\infty} = \sum_{k=1,2} \frac{\Delta\epsilon_k}{[1 + (i\omega\tau_k)^{\alpha_k}]^{\beta_k}} - i \frac{\sigma_{dc}}{\omega\epsilon_0}, \quad (9)$$

where ϵ_{∞} is the extrapolated high-frequency permittivity, $\Delta\epsilon_k$ is the strength of the corresponding relaxation mode, and σ_{dc} is the dc conductivity. The relaxation time τ_k is related to the frequency of maximum loss through the parameters α_k and β_k , which describe the width and the asymmetry of the relaxation spectra, respectively ($\alpha = \beta = 1$ corresponds to a simple Debye-like process). As an example, fittings for both director alignments are given in Figs. 7(b) ($\perp\mathbf{n}$, N), 7(c) ($\perp\mathbf{n}$, N_{TB}), 8(b) ($\parallel\mathbf{n}$, N), and 8(c) ($\parallel\mathbf{n}$, N_{TB}). Measurement results were fitted by assuming two relaxation processes,

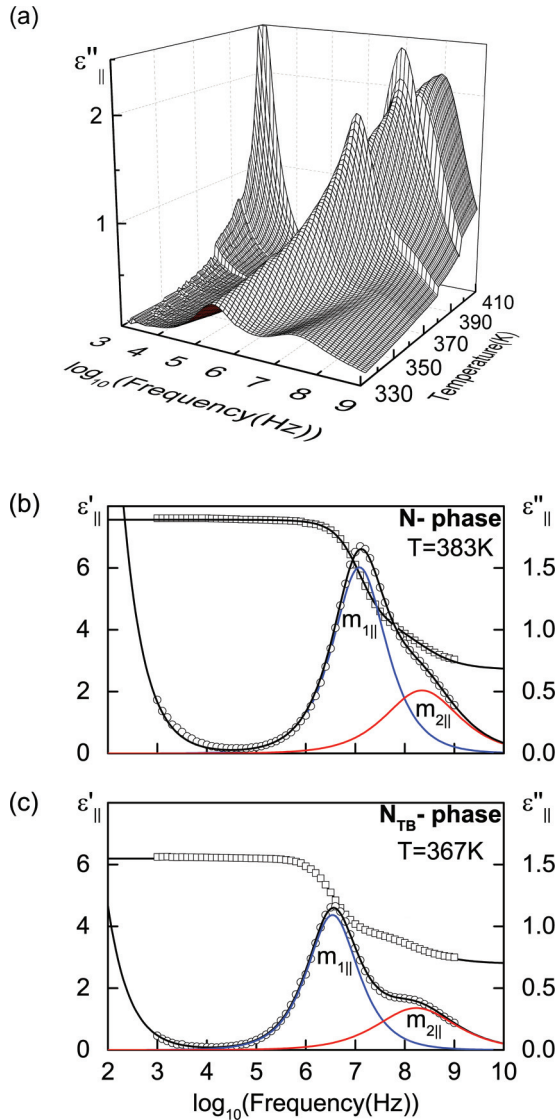


FIG. 8. (Color online) Parallel alignment. (a) Three-dimensional plot of the dielectric losses vs temperature and logarithm of the frequency. Frequency dependence of $\epsilon'_{||}$ (\square) and $\epsilon''_{||}$ (\circ) (b) in the N phase and (c) in the N_{TB} phase. In (b) and (c) solid lines are fits to Eq. (9).

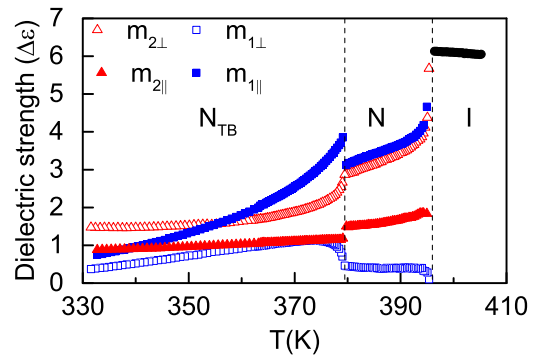


FIG. 9. (Color online) Dielectric strength of the relaxation modes vs temperature: full symbols, parallel alignment, empty symbols, perpendicular alignment; (\star) isotropic phase, ($\blacksquare, \blacklozenge$) low-frequency mode in the N and N_{TB} phases, ($\blacktriangle, \blacktriangleleft$) high-frequency mode in the N and N_{TB} phases.

mode strength ($\Delta\epsilon_{m1||}$) implies a much steeper reduction of the static permittivity than that found in the glass cells [see Fig. 6(a)]. As we have already indicated, this behavior is attributed to the inhomogeneous director distribution caused by electroconvective instabilities.

As already noted for CB7CB [2], at the N - N_{TB} transition, on lowering the temperature, the contribution of the low-frequency mode ($m_{1\perp}$) to the perpendicular component of the permittivity shows an abrupt increase. This is clear from Figs. 7(a) and 9, where the strength of the low-frequency mode ($m_{1\perp}$) shows a rapid increase below the N - N_{TB} transition. Such a sharp growth can be explained by the sudden tilt of the average axis of the longitudinal dipole moment, compatible with the heliconical director distribution. The dielectric strengths are obtained from a deconvolution of the frequency dependent dielectric response, as indicated in Fig. 7, and because of this it is not possible to determine if the apparent change in the strength is discontinuous or continuous, but the change in the appearance of the spectra is dramatic. Meanwhile, the strength of the predominant mode $m_{2\perp}$ undergoes a small decrease at the transition and then reduces more slowly at lower temperatures. Regarding the parallel configuration, the low-frequency contribution experiences an increase at the N - N_{TB} transition and the resulting value of the static permittivity is almost the same as that obtained with glass cells and ac voltages [see Fig. 6(a), full symbols]. A simple and tentative explanation for this behavior can be given in terms of the sharp decrease of the sample conductivity at the transition to the twist-bend nematic phase, which will hinder director fluctuations and allow for the realignment of the director parallel to the field.

An Arrhenius plot of the temperature dependence of the characteristic relaxation frequencies associated with each mode is given in Fig. 10. The analysis of these relaxation frequencies yields another interesting observation. While the dielectric amplitudes of the relaxation processes experience clear jumps at the N - N_{TB} transition, the corresponding frequencies remain almost unaltered showing a slight decrease for the end-over-end rotation and a comparable increase for the high-frequency mode. In addition, the activation energy for the end-over-end process is found to be almost unaltered

approximately a Cole-Cole shape, having α about 0.95 for m_1 and 0.75 for m_2 in both nematic phases.

Dielectric strengths for each relaxation are given as a function of temperature in Fig. 9. As observed also in the three-dimensional plot (see Fig. 7), for the perpendicular component of the permittivity, the high-frequency mode ($m_{2\perp}$) dominates over the temperature range of the nematic phase. There is a minor contribution from the low-frequency mode ($m_{1\perp}$), but its very low strength allows us to attribute it to a very small amount of director misalignment in the planar configuration. Conversely, for the parallel alignment the dielectric spectrum is dominated by the low-frequency relaxation ($m_{1||}$, end-over-end reorientation), with a smaller contribution from the high-frequency mode ($m_{2||}$) (see Fig. 9). Although this behavior would be expected for the parallel director configuration, the rapid decrease of the low-frequency

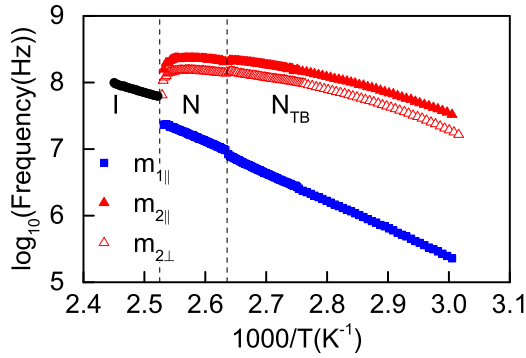


FIG. 10. (Color online) Arrhenius plot of the frequency of the relaxation modes: full symbols, parallel alignment, empty symbols, perpendicular alignment; (•) isotropic phase, (■) low-frequency mode in the N and N_{TB} phases, (▲, △) high-frequency mode in the N and N_{TB} phases.

due to convective instabilities in the nematic phase already discussed. Neglecting any changes in the orientational order parameter at the N - N_{TB} transition, this gives a tilt angle of 30° for CB9CB in the twist-bend phase 6 K below the N - N_{TB} transition, similar to that already reported for CB7CB [17,37].

2. Elastic constants from electric-field induced realignment

As Dozov proposed theoretically [12], spontaneous stabilization of the predicted lower local symmetry nematic phases with splay-bend or twist-bend modulation can result from a negative bend coefficient K_3 . In addition, it was shown that the difference in the elastic free energy between the two possible modulated nematic mesophases imposes the inequality $K_1 > 2K_2$ for the splay and twist elastic constants in order for the twist-bend distortion to be energetically favorable with respect to the splay-bend phase. Therefore, investigations of the elastic properties are directly related to the experimental identification of such spontaneously modulated nematic phases. In order to explore the possible stabilization of a twist-bend nematic phase, a number of studies have examined the elastic properties of the higher temperature nematic phase [6,7,9,46] for materials that exhibit the twist-bend nematic phase. These include (i) molecular-field calculations for the shorter dimer, CB7CB, suggesting that the condition $K_1 > 2K_2$ is fulfilled [2] and (ii) experimental determination of splay and bend elastic constants, but not the twist elastic constant, for the nearest longer dimer CB11CB [6]. In Ref. [46] measurements of K_1 , K_2 , and K_3 for CB7CB in both the nematic and the twist-bend nematic phases are reported. The value they found for the ratio K_1/K_2 was around 1.4 in the N phase but the most intriguing result is the huge increase of K_3 and the decrease of K_1 on entering the N_{TB} phase. This is explained as being due to a different nature of the elastic distortions near the N_{TB} - N phase transition [46].

We have determined the splay and bend elastic constants in the nematic phase of CB9CB by measuring the change in the capacitance when a variable voltage is applied to planar aligned samples of the nematic director. The frequency of the applied electric field was set equal to 5 kHz, as for measurements of the static permittivity, to avoid undesired ionic effects. Careful analysis of the data was performed at a series of temperatures by fitting the capacitance vs voltage curve to the following equations [47]:

$$V = \frac{2V_{th}}{\pi} \sqrt{1 + \gamma\eta} \int_{\psi_0}^{\pi/2} \left[\frac{1 + \kappa\eta\sin^2\psi}{(1 + \gamma\eta\sin^2\psi)(1 - \eta\sin^2\psi)} \right]^{1/2} d\psi, \quad (10a)$$

$$C = C_{\perp} \frac{\int_{\psi_0}^{\pi/2} \left[\frac{(1 + \gamma\eta\sin^2\psi)(1 + \kappa\eta\sin^2\psi)}{(1 - \eta\sin^2\psi)} \right]^{1/2} d\psi}{\int_{\psi_0}^{\pi/2} \left[\frac{1 + \kappa\eta\sin^2\psi}{(1 + \gamma\eta\sin^2\psi)(1 - \eta\sin^2\psi)} \right]^{1/2} d\psi}. \quad (10b)$$

Here the parameter η is related to the maximum tilt angle at the center of the cell ϕ_m through the relation $\eta = \sin^2(\phi_m)$; the parameters γ and κ correspond to the reduced quantities $\gamma = C_{\perp}/C_{\parallel} - 1$ and $\kappa = K_3/K_1 - 1$. The capacitance for perpendicular director alignment, C_{\perp} , was deduced from the capacitance of the cell before the onset of the Fréedericksz transition, V_{th} . The capacitance for parallel director alignment,

at the transition, being about 76 kJ mol^{-1} in both nematic phases.

Recent studies on CB7CB [17,37] reported values of the tilt angle of the director, estimated from birefringence measurements. In the heliconical N_{TB} phase, the tilt angle shows a very steep increase near the phase transition which is followed by a less rapid increase when it reaches more than 35° at just over 50°C below the N - N_{TB} transition [37]. Similar values are estimated from ^2H NMR results for CB7CB [21]. However, more recent NMR studies of CB7CB using ^{129}Xe as a spin probe based on a recently proposed model for the analysis of the chemical shift shows that the conical angle exhibits a less rapid increase on entering the N_{TB} phase [45]. This is a puzzling observation to which we shall return shortly. In our dielectric characterization of the twist-bend nematic phase, we claim that the observation of a sudden increase in the contribution of the low-frequency (end-over-end) relaxation $m_{1\perp}$ to the measured perpendicular dielectric absorption at the N - N_{TB} transition is consistent with the rapid development of a director tilt, which would be expected and has been seen on the formation of a heliconical phase. This, in principle, provides a method to estimate values of the tilt angle for CB9CB from our dielectric measurements.

For the purposes of estimating the tilt angle in the twist-bend nematic phase, we assume that the dielectric strength ($\Delta\varepsilon_{m_{1\perp}}$) of $m_{1\perp}$ in the twist-bend nematic phase is due only to the director tilt (θ_0) with respect to the heliconical axis, and that the order parameter does not change at the transition. Then the value of $\Delta\varepsilon_{m_{1\perp}}$ in the twist-bend phase is the appropriate component of the dielectric strength measured for this relaxation in the absence of tilt $\Delta\varepsilon_{m_{1\parallel}}$ rotated by the tilt angle; $\Delta\varepsilon_{m_{1\parallel}}$ is the dielectric strength as measured in the nematic phase ($\theta_0 = 0$), for the parallel component of the absorption. Since the components of the dielectric strength behave as second rank tensors, the relation between the value $\Delta\varepsilon_{m_{1\perp}}$ in the twist-bend phase measured perpendicular to the heliconical axis and the value for zero tilt $\Delta\varepsilon_{m_{1\parallel}}$ measured along the alignment axis is $\Delta\varepsilon_{m_{1\perp}} = \Delta\varepsilon_{m_{1\parallel}} \sin^2\theta_0$. At 6 K below the N - N_{TB} transition the value of $\Delta\varepsilon_{m_{1\perp}}$ is 1.1, while the value of $\Delta\varepsilon_{m_{1\parallel}}$ is 4. This value has been rescaled to take account of the small misalignment in the $50\text{-}\mu\text{m}$ metal cell

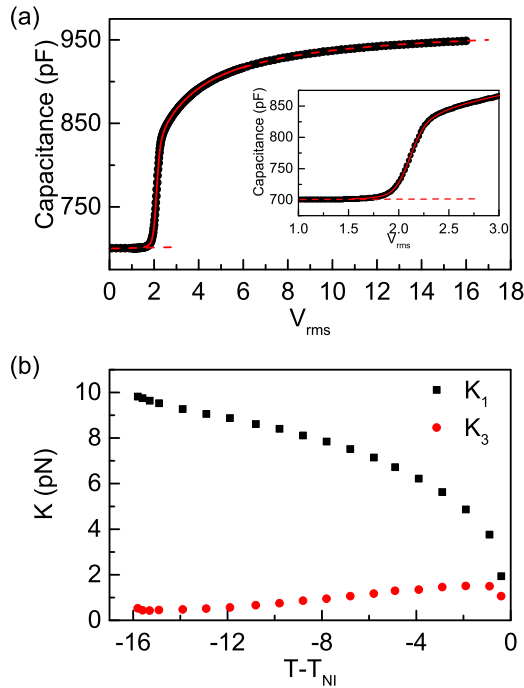


FIG. 11. (Color online) (a) Voltage dependence of the capacitance recorded at 5 kHz for the shifted temperature $T - T_{NI} = -13$ K. Solid line shows the theoretical fit to Eqs. (10a) and (10b). (b) Temperature dependence of the elastic constants K_1 and K_3 in the nematic phase.

791 $C_{||}$, was determined from the extrapolated capacitance in the
 792 limit of a very large aligning field $1/V \rightarrow 0$ [48]. In order to
 793 obtain the threshold voltage V_{th} and κ , capacitance data above
 794 the threshold voltage were fitted to Eqs. (10a) and (10b) based
 795 on a least squares minimization procedure. These values of
 796 V_{th} and κ were employed to calculate K_1 and K_3 using the
 797 relationship

$$K_1 = (V_{th}/\pi)^2 \varepsilon_0 \Delta \varepsilon. \quad (11)$$

798 Before fitting over the entire temperature range, tests for
 799 different values of the pretilt angle, α , in the range of $0^\circ - 3^\circ$,
 800 were performed by introducing in Eqs. (10a) and (10b) the
 801 integral limit value $\psi_0 = \arcsin[\sin \alpha / \sqrt{\eta}]$. Even though not
 802 too great a difference was observed, the best and final fittings
 803 were performed for $\alpha = 2.2^\circ$. An example of the voltage
 804 variation of the capacitance together with the corresponding
 805 fitting is plotted in Fig. 11(a) for a temperature close to the
 806 $N-N_{TB}$ transition.

807 The splay and bend elastic constants are shown in Fig. 11(b)
 808 as a function of temperature. The results show that the splay
 809 elastic constant, K_1 , increases with decreasing temperature
 810 while the bend elastic constant, K_3 , which is significantly
 811 smaller than K_1 , decreases with decreasing temperature, after
 812 an initial increase at the $N-I$ transition, reaching values as
 813 small as 0.43 pN, before increasing slightly as found for other
 814 systems [9]. Such a decrease is in good agreement with earlier
 815 theoretical predictions [11] and the results are comparable
 816 to experimental determinations for other odd liquid crystal
 817 dimers exhibiting a twist-bend nematic phase [9,10,15,49].
 818 The results for CB9CB recorded here, for both K_1 and K_3 ,

819 have slightly higher values than for the previously reported
 820 homologue CB7CB [25,49], but for the longer analogue
 821 CB11CB [6] both K_1 , but above all K_3 , are much higher.
 822 This difference may be attributed to the effect the length of the
 823 linking chain has on the molecular shape or also to a different
 824 experimental methodology. The shorter chains for CB9CB
 825 and CB7CB would enhance the bent molecular structure of
 826 the dimer with respect to that of the undecane homologue,
 827 significantly reducing K_3 . Our measurements for CB7CB [49]
 828 in the N phase are comparable to those reported in Ref. [46] for
 829 K_1 , but our value for K_3 near the N_{TB} phase is slightly larger
 830 (0.43 pN vs 0.3 pN) and of the same order as for CB9CB. It is
 831 important to note that in the analysis, the splay elastic constant
 832 depends on the assumed value for the dielectric anisotropy
 833 at the measurement frequency. This was carefully selected to
 834 avoid spurious low-frequency ionic contributions that tend to
 835 increase the permittivity and thus to overestimate K_1 values.

836 The temperature dependence of K_3 , and in particular its
 837 maximum near T_{NI} , require further analysis. Similar behavior
 838 has been found for liquid crystal mixtures of bent-core and
 839 rodlike molecules with a sufficiently high concentration of
 840 bent-core molecules [50,51]. As proposed in these cases, the
 841 initial increase of K_3 could be related to the increase of
 842 the order parameter, whereas its further decrease would arise
 843 from the better coupling of the bent shape of the molecules
 844 to a bend distortion of the director, depending on the bend
 845 angle. However, for liquid crystal dimers it is important
 846 to recall that the internal flexibility of the molecules leads
 847 to a temperature dependent conformational distribution. The
 848 similarity between the dielectric anisotropy [Fig. 6(b)] and the
 849 bend elastic constant [Fig. 11(b)] supports the assumption that
 850 the temperature dependence of the conformational distribution
 851 should not be disregarded when analyzing the behavior of K_3 .

C. ^2H NMR spectroscopy: Chirality, order parameters, and conical angle

852 The aim of the NMR experiments is to explore the orien-
 853 tational order of both nematic phases, and for the twist-bend
 854 nematic phase its chirality and conical angle, and how they
 855 vary with temperature. A selection of deuterium NMR spectra
 856 is shown in Fig. 12. In the nematic phase at 380 and 377 K
 857 the spectra show a single quadrupolar doublet consistent with
 858 the achirality of the phase and the alignment of the director by
 859 the magnetic field. Careful examination of the spectra reveals
 860 a weak quadrupolar doublet which has been associated with
 861 a partially deuterated dimer impurity; this single doublet is
 862 more apparent in the N_{TB} phase [45]. For the spectrum in the
 863 nematic phase at 377 K the spectral lines broaden slightly,
 864 consistent with the approach of the N_{TB} phase with its higher
 865 viscosity. In the twist-bend nematic phase the two spectra
 866 at 376 and 363 K contain two quadrupolar doublets which
 867 provide a clear demonstration of the phase chirality, to be
 868 discussed later. The spectra were measured carefully on going
 869 through the $N_{TB}-N$ phase transition, and the change in the
 870 spectral linewidths is consistent with a weak first-order phase
 871 transition and an almost continuous change in the mean of the
 872 prochiral quadrupolar splittings.

873 The temperature variation of the quadrupolar splittings
 874 for the probe CB7CB- d_4 dissolved in the dimer CB9CB are
 875
 876

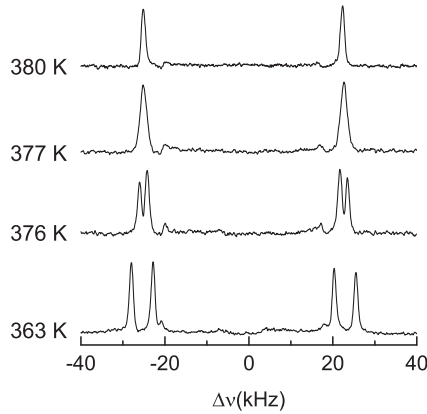


FIG. 12. The ^2H NMR spectra of $\text{CB7CB-}d_4$ dissolved in CB9CB at four temperatures, two in the nematic phase and the lower two in the twist-bend nematic phase.

877 shown in Fig. 13. Although the splittings are for the probe, its
 878 low concentration and structural similarity to the host should
 879 ensure that they reflect the orientational order of CB9CB . In
 880 the N phase we see the initial, normal growth of this order with
 881 decreasing temperature. As the N_{TB} phase is approached, so the
 882 rate of increase diminishes and the splitting essentially reaches
 883 a plateau which is unusual [9]. On entering the twist-bend
 884 nematic two doublets are clearly apparent, and this loss of
 885 equivalence of the prochiral deuterons results from the loss of
 886 the plane of symmetry in the averaged molecule caused by the
 887 chirality of the low temperature nematic phase (see Fig. 14)
 888 [2]. This provides a clear indication of the identity of the N_{TB}
 889 phase. The difference in the two quadrupolar splittings grows
 890 with decreasing temperature and might be associated with a
 891 change in the N_{TB} phase structure. However, molecular-field
 892 theory predicts that although the pitch decreases rapidly in the
 893 N_{TB} phase after the transition, it then changes relatively slowly
 894 at lower temperatures [26]. In marked contrast to the behavior
 895 of this chiral splitting the mean quadrupolar splitting is more
 896 or less independent of temperature. To understand this, at least
 897 qualitatively, we recall that with decreasing temperature the
 898 orientational order should grow, as should the conical angle.
 899 Whereas the increasing order causes the quadrupolar splitting
 900 to increase, increasing the conical angle results in a decrease of

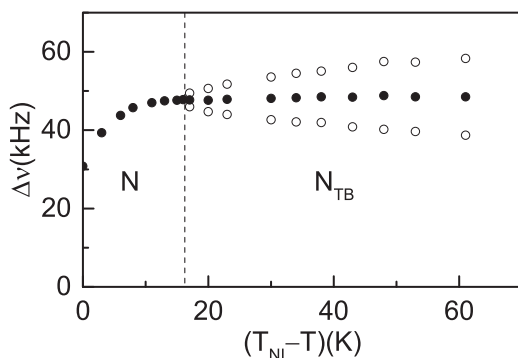


FIG. 13. The dependence on the shifted temperature, $T_{\text{NI}} - T$, of the quadrupolar splittings for the probe, $\text{CB7CB-}d_4$, doped in the nematic and twist-bend nematic phases of the host, CB9CB .

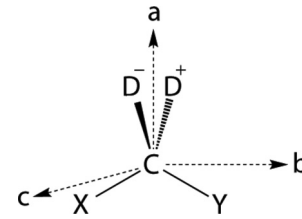


FIG. 14. The conformationally averaged structure of $\text{CB7CB-}d_4$ with the reference frame set in one of the methylene, CD_2 , fragments. The coordinate system a, b, c is also shown together with the averaged groups X (in the spirit of the model the X cyanobiphenyl group is not averaged because C-X is parallel to the para-axis of the cyanobiphenyl group also known as cyanobiphenyl) and Y (also known as the spacer and second cyanobiphenyl group). The mirror plane at the methylene group is in the plane of the paper, i.e., the plane defined by XCY . In a chiral environment, such as a twist-bend nematic, this symmetry plane is removed, and the atoms D^+ and D^- , above and below the plane of the paper, become inequivalent.

the splitting. It seems that these two effects essentially balance
 throughout the N_{TB} phase as can be seen in Fig. 15.

A more quantitative interpretation of the NMR splittings
 can be obtained by relating them to the Saupe ordering matrix
 for the CB7CB dimer, details of which have been given by
 Beguin *et al.* [18]. The rigid fragments containing the prochiral
 deuterons are in the first and last methylene groups in the
 heptane spacer, which for $\text{CB7CB-}d_4$ are equivalent. These
 are now used as reference frames and allow us to include the
 molecular flexibility associated with the spacer. By taking an
 average over all molecular conformers, the system can be
 treated as the averaged structure sketched in Fig. 14. Attached
 to the carbon atom of a CD_2 unit are two nonequivalent groups:
 X represents a cyanobiphenyl group, while Y is the methylene
 spacer attached to the second terminal cyanobiphenyl group
 averaged over all conformers. The plane formed by $X, C,$ and
 Y is a mirror plane and the c axis is orthogonal to this; the
 a axis bisects the D^+CD^- bond angle and is orthogonal to
 c ; the b axis is orthogonal to a and c . In this frame the
 Saupe ordering matrix, which we shall refer to as the averaged
 Saupe matrix, takes the form

$$\mathbf{S} = \begin{pmatrix} S_{aa} & S_{ab} & 0 \\ S_{ab} & S_{bb} & 0 \\ 0 & 0 & S_{cc} \end{pmatrix}. \quad (12)$$

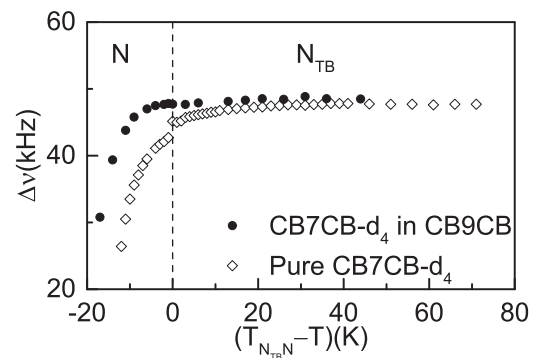


FIG. 15. The variation of the mean quadrupolar splitting with the shifted temperature, $T_{\text{NTB},N} - T$, for $\text{CB7CB-}d_4$ doped in CB9CB (\bullet) and for $\text{CB7CB-}d_4$ (\diamond).

922 The key quantities of relevance here are the quadrupolar
923 splittings for the two deuterons and these are

$$\Delta\nu_+ = (3/2)q_{CD}S_{CD+}, \quad (13a)$$

$$\Delta\nu_- = (3/2)q_{CD}S_{CD-}, \quad (13b)$$

924 where q_{CD} is the component of the quadrupolar tensor
925 parallel to the C-D bond, assuming the local symmetry to be
926 cylindrically symmetric about the bond. Because of the mirror
927 plane symmetry, the order parameters for the two C-D bonds
928 denoted S_{CD+} and S_{CD-} are equal, and Beguin *et al.* [18] have
929 shown that these two order parameters can be written in terms
930 of the elements of the averaged Saupe matrix as

$$S_{CD+} = S_{aa}\cos^2\beta + S_{cc}\sin^2\beta = S_{CD-}, \quad (14)$$

931 where β is the angle between a C-D bond and the a axis.
932 The quadrupolar splitting measured in the nematic phase is
933 proportional to two diagonal elements of the Saupe matrix and
934 one of these, S_{cc} , is a principal component.

935 The chirality of the twist-bend nematic phase means that the
936 mirror plane for the methylene group is lost and all elements
937 of the averaged matrix are nonzero. Of particular significance
938 is the off-diagonal element S_{ac} , as a result of which the two
939 C-D bonds are no longer equivalent and the relevant order
940 parameters are now

$$S_{CD+} = S_{aa}\cos^2\beta + S_{cc}\sin^2\beta + S_{ac}\sin 2\beta, \quad (15a)$$

$$S_{CD-} = S_{aa}\cos^2\beta + S_{cc}\sin^2\beta - S_{ac}\sin 2\beta. \quad (15b)$$

941 The label $+$ or $-$ is seen to relate to the sign of the term
942 in S_{ac} in the expression for the order parameters of the C-D
943 bonds. We can see that by taking the mean of the quadrupolar
944 splittings in the N_{TB} phase then via Eqs. (13) and (15) this sum
945 is given by

$$(\Delta\nu_+ + \Delta\nu_-)/2 = (3/4)q_{CD}(S_{aa}\cos^2\beta + S_{cc}\sin^2\beta), \quad (16)$$

946 which is equivalent to the quadrupolar splitting in the nematic
947 phase [see Eq. (14)]. It is then the mean splitting in the N_{TB}
948 phase which should be compared with the splitting in the
949 nematic phase as we have done in Fig. 15. The results, shown
950 in Eqs. (15a) and (15b), also indicate that the off-diagonal
951 element, S_{ac} , is related to the difference in the quadrupolar
952 splittings by

$$(\Delta\nu_+ - \Delta\nu_-)/2 = (3/4)q_{CD}S_{ac}\sin 2\beta. \quad (17)$$

953 We refer to this difference as the chiral splitting, and it is
954 zero in an achiral system, for which the off-diagonal element
955 S_{ac} of the averaged Saupe matrix vanishes.

956 In Figs. 15 and 16, the results for the mean quadrupolar
957 splitting and the chiral quadrupolar splitting, respectively, for
958 CB7CB- d_4 dissolved in CB9CB are compared with those for
959 pure CB7CB- d_4 [2]. Since the two systems have different
960 transition temperatures, we have used a shifted temperature
961 scale with respect to the transition temperature, $T_{N_{TB}N}$. The
962 results for CB7CB- d_4 dissolved in CB9CB clearly show
963 that the splitting in the nematic phase is almost continuous
964 with the mean splitting in the twist-bend nematic as well with
965 as the pretransitional plateau in the nematic phase prior to the
966 formation of the N_{TB} phase. This behavior is in contrast to
967 that of the lower homologue CB7CB, where there is a clear
968 discontinuity in the splittings for the two phases. This suggests

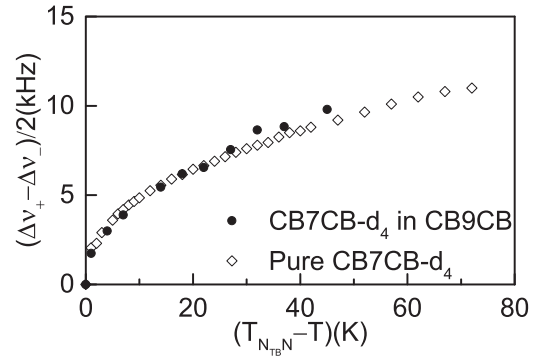


FIG. 16. The variation of the chiral quadrupolar splitting with the shifted temperature, $T_{N_{TB}N} - T$, for CB7CB- d_4 doped in CB9CB (●) and for CB7CB- d_4 (◇).

969 that the first-order $N_{TB} - N$ transition for CB7CB is stronger
970 than that for CB9CB, which is much closer to second order,
971 for which there would be no discontinuity. The strength of this
972 transition may be related to the length of the N phase prior
973 to the formation of the N_{TB} phase analogous to the behavior
974 of the Sm-A- N transition [52]. In Fig. 16, the temperature
975 dependence of the chiral splitting for CB9CB is compared
976 with that for its shorter homologue CB7CB. On the shifted
977 temperature scale, the results are very similar, except that the
978 chiral splitting is apparently zero, to within experimental error,
979 for CB9CB at the transition temperature $T_{N_{TB}N}$, while there is
980 a small but significant jump for CB7CB indicating a difference
981 in the strength of the transition for the two dimers. This
982 difference may well result from the change in the curvature
983 of their average structures [26].

984 The two prochiral quadrupolar splittings of the probe
985 molecule 8CB- d_2 dissolved in CB7CB have been used to
986 estimate the helical pitch of the host and the conical angle
987 of the director [21]. This determination is based on a model
988 for the director distribution in the N_{TB} phase, its relation to
989 the molecular conformation to give the orientational order and
990 the quadrupolar splittings of the prochiral deuterons. More
991 recently ^{129}Xe has been used as an NMR probe to explore
992 the structure of the N and N_{TB} nematic phases for CB7CB
993 [45]. This experiment yields a single peak which gives the
994 shielding or chemical shift and a model has been developed
995 to determine both the conical angle and the orientational
996 order parameter of the cyanobiphenyl group with respect to
997 the director. To achieve this, analytic expressions have been
998 proposed to describe the temperature dependence in the N_{TB}
999 phase of the orientational order parameter and the conical
1000 angle. Here we shall use the same approach to obtain this
1001 information from the mean quadrupolar splitting for the probe
1002 CB7CB- d_4 in CB9CB.

1003 To understand how the probe molecule CB7CB- d_4 used in
1004 our NMR experiments is ordered, it is helpful to envisage the
1005 conformational average it will adopt on the NMR time scale.
1006 It has been thought that the average shape of an odd dimer
1007 would have a bent core, especially as this is required for the
1008 formation of the twist-bend nematic phase [37]; indeed this
1009 approximates to the average shape that has been calculated for
1010 odd dimers [53]. However, when the averages of properties
1011 such as the quadrupolar splittings are considered then it is

1012 necessary to calculate the averaged shape in the frame relevant
 1013 to that property, in other words, in the frame where the property
 1014 does not change with the molecular conformation. For the
 1015 deuterons localized in the terminal positions of the spacer in
 1016 CB7CB- d_4 the natural frame would be with the major axis
 1017 parallel to the para-axis of the cyanobiphenyl group. The
 1018 conformational average would leave one cyanobiphenyl group
 1019 of CB7CB unchanged but the averaged spacer and second
 1020 mesogenic group should result in a uniaxial object parallel
 1021 to the first mesogenic group containing the reference frame
 1022 [54,55]. The order parameter for the para-axis with respect to
 1023 the magnetic field, S_p , can be determined from the quadrupolar
 1024 splittings of the prochiral deuterons via

$$S_p(T) = (2/3)|\Delta\nu(T)|q_{CD}P_2(\cos\gamma), \quad (18)$$

1025 where γ is the angle between a C-D bond and the para-axis.
 1026 This is taken to be the tetrahedral angle 109.47° and the
 1027 quadrupolar coupling constant, q_{CD} , is set equal to 168 kHz.
 1028 The model gives the order parameter, $|S_p(T)|$, with respect to
 1029 the helix axis as

$$|S_p(T)| = |S_p^n(T)P_2[\cos\theta_0(T)]|, \quad (19)$$

1030 where S_p^n is also that for the para-axis but with respect to the
 1031 director. The model of Jokisaari *et al.* [45] assumes specific
 1032 temperature dependences for S_p^n and θ_0 which allow Eq. (19)
 1033 to be written as

$$|S_p(T)| = |(1 - yT/T_{N_{TB}N})^z P_2[\cos[\theta(0)(1 - y_\theta T/T_{N_{TB}N})^\beta]]|, \quad (20)$$

1034 where y and z are fitting parameters and y allows for the order
 1035 parameter to be nonzero at the phase transition. Similarly $\theta(0)$,
 1036 y_θ , and β are fitting parameters for the conical angle; $\theta(0)$ is
 1037 that at absolute zero; and y_θ allows for the conical angle to
 1038 be nonzero at the transition. Thus, in principle, this model can
 1039 yield values for the order parameter of the mesogen in the N_{TB}
 1040 phase as well as the conical angle from measurements of the
 1041 mean splitting as a function of temperature.

1042 The determination of the five parameters of the model from
 1043 a limited data set presents a challenge. To simplify this a
 1044 little we note that the mean splitting is almost continuous at
 1045 the nematic to twist-bend nematic transition, and accordingly
 1046 we assume that the conical angle is zero at the transition and
 1047 the parameter y_θ is set equal to unity. However, y is not equal
 1048 to 1 because the orientational order parameter, S_p^n , does not
 1049 vanish at the transition. With these constraints, and within
 1050 the experimental accuracy of the chiral splittings, we have
 1051 fitted our measurements to the model using a least squares
 1052 procedure [45]. The order parameters calculated in this way
 1053 from the mean quadrupolar splittings, via Eq. (18), are shown
 1054 as a function of the reduced temperature in Fig. 17(a). From
 1055 the fitting, we have obtained the following values for the
 1056 parameters of the model proposed by Jokisaari *et al.* [45]:
 1057 $y = 0.919$, $z = 0.223$, $\theta(0) = 42.5^\circ$, and $\beta = 0.374$. From
 1058 the limited data set available, it is not possible to determine
 1059 the uncertainties associated with these derived parameters, but
 1060 these values allow us to calculate the order parameter for the
 1061 para-axis of the cyanobiphenyl group and the conical angle in
 1062 the twist-bend nematic phase.

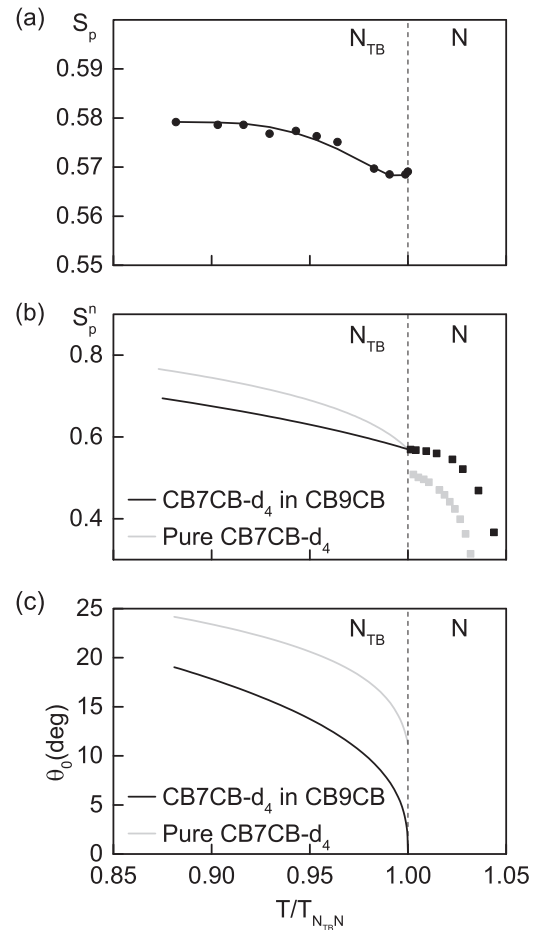


FIG. 17. (a) The dependence of the order parameter, S_p , on the reduced temperature in the twist-bend nematic phase, both experimental (\bullet) and calculated (---). (b) The dependence of the orientational order parameter for the para-axis of the cyanobiphenyl group, S_p^n , for CB7CB- d_4 in CB9CB on the reduced temperature in the twist-bend nematic (indirect ---) and nematic (direct \blacksquare) together with comparable results for pure CB7CB- d_4 (indirect ---) and nematic (direct \blacksquare) [45]. (c) The dependence of the conical angle, θ_0 , in the twist-bend nematic phase on the reduced temperature for CB7CB- d_4 in CB9CB (---) and for pure CB7CB- d_4 (---) [45].

Our results for the order parameters S_p^n in the N_{TB} phase 1063
 as a function of the reduced temperature, $T/T_{N_{TB}N}$, are shown 1064
 as solid lines in Fig. 17(b). There appears to be a more or 1065
 less linear increase in the order parameter with decreasing 1066
 temperature. For comparison we also show results obtained 1067
 in the same way for pure CB7CB- d_4 [45]. In addition we show 1068
 in Fig. 17(b) the order parameters determined directly from 1069
 the quadrupolar splittings in the nematic phase. The order 1070
 parameter in the nematic phase is greater for CB9CB than for 1071
 pure CB7CB. This difference is likely to result from the greater 1072
 anisotropy or smaller curvature of CB9CB caused by its longer 1073
 spacer. The other clear difference in behavior between the two 1074
 dimers is the gradient in the order parameters prior to the 1075
 N_{TB} - N transition; for CB9CB this is shallow but steeper for 1076
 CB7CB. The most striking feature is the difference in the order 1077
 parameters between the two nematic phases. Thus for CB9CB 1078
 the order parameter is continuous, to within experimental error, 1079

at the transition, but for CB7CB there is a strong jump in the order parameter at the N_{TB} - N transition showing a clear difference to the behavior of CB9CB. The Landau-like theory of Dozov [12] and the molecular theory of Greco *et al.* [26] both predict that the transition should be continuous.

We conclude with our results for the conical angle which is one of the defining characteristics of the twist-bend nematic phase. The values found for CB9CB are shown as a function of the reduced temperature in Fig. 17(c). Our experimental results for the mean splitting of the probe CB7CB- d_4 in CB9CB suggest that the N_{TB} - N transition is essentially continuous, and the conical angle is zero at the transition. In Fig. 17(c) we compare these results with those found for pure CB7CB using the same methodology [45]. It is clear that the dimer CB7CB appears to have a larger conical angle than its longer homologue CB9CB, which may be due to differences in the nature of the N_{TB} - N transition for the two dimers. The conical angles obtained from ^2H NMR mean splittings seem to be smaller than those estimated using other techniques, and so it may be useful to explore the use of different spin probes in the NMR experiments.

IV. CONCLUDING REMARKS

In summary, we have presented dielectric, calorimetric, and ^2H NMR studies on CB9CB. As expected, the properties of this odd liquid crystal dimer are similar to those of its shorter analogue CB7CB, but a more detailed analysis of the results provides more evidence concerning the structure of the twist-bend nematic phase for these cyanobiphenyl dimers with odd spacers. We have also shown that for CB9CB, high enough cooling rates prevent its crystallization and the N_{TB} mesophase becomes a twist-bend nematic glassy state.

The parallel component of the static dielectric permittivity reflects the phase transitions and shows a continuous decrease on cooling after entering the nematic phase which reflects the temperature dependence of the conformational distribution. This decrease leads to a decrease of the dielectric anisotropy which changes sign from positive to negative in the N_{TB} phase. The tilt of the director in the heliconical phase also plays a role in the sign change of the dielectric anisotropy. The appearance of tilt at the N - N_{TB} phase transition is clearly visible in dielectric experiments, similar to what was reported for CB7CB [2]. The contribution of the low-frequency mode to the perpendicular component of the permittivity shows an abrupt increase that can be explained by the rapid development of a director tilt of the average axis of the longitudinal dipole moment associated with the director.

The elastic constants K_1 and K_3 in the high temperature nematic phase of CB9CB show a behavior that is similar

to that for other bent-shaped compounds: The splay elastic constant is larger than the bend elastic constant, and the latter decreases with decreasing temperature towards almost zero on approaching the N_{TB} phase. There is, however, a small increase in K_3 just prior to the formation of the N_{TB} phase as found for other odd dimers. Finally heat-capacity data measurements have allowed us to characterize the N_{TB} - N phase transition as first order, although nearly tricritical.

Our results confirm that the mesogenic dimer CB9CB forms a twist-bend nematic phase, as do other members of the homologous series. The properties of the N_{TB} phase of CB9CB are similar to those measured for its shorter homologue CB7CB, though the nature of the phase transition from nematic to twist-bend nematic appears to differ for the two homologues. Calorimetric measurements confirm that this transition in both materials is first order, though it is much closer to second order for the longer homologue CB9CB. ^2H NMR results also point to the weaker first-order character of the N_{TB} - N phase transition for CB9CB compared with CB7CB; for example, the chiral splitting for CB9CB, which provides clear evidence for the assignment of the N_{TB} phase, is almost continuous through the transition whereas for CB7CB this has a clear discontinuity. The analysis of the mean quadrupolar splitting allows the orientational order and conical angle to be estimated approximately throughout the N_{TB} phase; these contrast with the behavior of CB7CB which has a larger order and tilt angle than for CB9CB.

The results presented in this paper and other referenced work show that the introduction of core flexibility into mesogens can have a dramatic effect on both the properties and phase behavior of the materials. The appearance of second nematic phase is perhaps the most dramatic consequence of the odd parity of the spacer combined with its flexibility in the cyanobiphenyl alkane dimers, but what is also remarkable is that the properties and nature of the phase transitions are critically dependent on the length of the methylene spacer, and by implication on the details of the chain flexibility. This adds a new dimension to the exploration of structure-property relationships for liquid crystal materials, and shows that in addition to their averaged bent shape and functionality the internal flexibility of mesogens is an important factor in determining their intriguing liquid crystal behavior.

ACKNOWLEDGMENTS

The authors are grateful for financial support from the MICINN project MAT2012-38538-C03-02,03 and from the Eusko Jaurlaritza-Gobierno Vasco (GI/IT-449-10). The authors also acknowledge the recognition from the Generalitat de Catalunya of GRPFM as Emergent Research Group (2009-SGR-1243).

- [1] V. P. Panov, M. Nagaraj, J. K. Vij, Y. P. Panarin, A. Kohlmeier, M. G. Tamba, R. A. Lewis, and G. H. Mehl, *Phys. Rev. Lett.* **105**, 167801 (2010).
- [2] M. Cestari, S. Diez-Berart, D. A. Dunmur, A. Ferrarini, M. R. de la Fuente, D. J. B. Jackson, D. O. López, G. R. Luckhurst, M. A. Pérez-Jubindo, R. M. Richardson, J. Salud, B. A. Timimi, and H. Zimmermann, *Phys. Rev. E* **84**, 031704 (2011).
- [3] P. A. Henderson and C. T. Imrie, *Liq. Cryst.* **38**, 1407 (2011).

- [4] C. S. P. Tripathi, P. Losada-Pérez, C. Glorieux, A. Kohlmeier, M. G. Tamba, G. H. Mehl, and J. Leys, *Phys. Rev. E* **84**, 041707 (2011).
- [5] M. Sepelj, A. Lesac, S. Baumeister, S. Diele, H. L. Nguyen, and D. W. Bruce, *J. Mater. Chem.* **17**, 1154 (2007).
- [6] R. Balachandran, V. P. Panov, J. K. Vij, A. Kocot, M. G. Tamba, A. Kohlmeier, and G. H. Mehl, *Liq. Cryst.* **40**, 681 (2013).

- [7] V. Borshch, Y.-K. Kim, J. Xiang, M. Gao, A. Jáklí, V. P. Panov, J. K. Vij, C. T. Imrie, M. G. Tamba, G. H. Mehl, and O. D. Lavrentovich, *Nat. Commun.* **4**, 2635 (2013).
- [8] D. O. López, N. Sebastián, M. R. de la Fuente, J. C. Martínez-García, J. Salud, M. A. Pérez-Jubindo, S. Diez-Berart, D. A. Dunmur, and G. R. Luckhurst, *J. Chem. Phys.* **137**, 034502 (2012).
- [9] K. Adlem, M. Čopič, G. R. Luckhurst, A. Mertelj, O. Parri, R. M. Richardson, B. D. Snow, B. A. Timimi, R. P. Tuffin, and D. Wilkes, *Phys. Rev. E* **88**, 022503 (2013).
- [10] K. L. Atkinson, S. M. Morris, F. Castles, M. M. Qasim, D. J. Gardiner, and H. J. Coles, *Phys. Rev. E* **85**, 012701 (2012).
- [11] M. Cestari, E. Frezza, A. Ferrarini, and G. R. Luckhurst, *J. Mater. Chem.* **21**, 12303 (2011).
- [12] I. Dozov, *Europhys. Lett.* **56**, 247 (2001).
- [13] P. J. Barnes, A. G. Douglass, S. K. Heeks, and G. R. Luckhurst, *Liq. Cryst.* **13**, 603 (1993).
- [14] S. M. Shamid, S. Dhakal, and J. V. Selinger, *Phys. Rev. E* **87**, 052503 (2013). It should be mentioned that recently a distinction has been made between the bare bend elastic constant K_3 and the renormalized coefficient K_{eff}^3 arising from Landau expansion, with the bare K_3 being always positive and K_{eff}^3 the negative constant examined by Dozov.
- [15] N. Sebastián, D. O. López, B. Robles-Hernández, M. R. de la Fuente, J. Salud, M. A. Pérez-Jubindo, D. A. Dunmur, G. R. Luckhurst, and D. J. B. Jackson, *Phys. Chem. Chem. Phys.* **16**, 21391 (2014).
- [16] R. J. Mandle, E. J. Davis, C. T. Archbold, S. J. Cowling, and J. W. Goodby, *J. Mater. Chem. C* **2**, 556 (2014).
- [17] P. K. Challa, V. Borshch, O. Parri, C. T. Imrie, S. N. Sprunt, J. T. Gleeson, O. D. Lavrentovich, and A. Jáklí, *Phys. Rev. E* **89**, 060501 (R) (2014).
- [18] L. Beguin, J. W. Emsley, M. Lelli, A. Lesage, G. R. Luckhurst, B. A. Timimi, and H. Zimmermann, *J. Phys. Chem. B* **116**, 7940 (2012).
- [19] J. W. Emsley, M. Lelli, A. Lesage, and G. R. Luckhurst, *J. Phys. Chem. B* **117**, 6547 (2013).
- [20] J. W. Emsley, P. Lesot, G. R. Luckhurst, A. Meddour, and D. Merlet, *Phys. Rev. E* **87**, 040501 (R) (2013).
- [21] C. Greco, G. R. Luckhurst, and A. Ferrarini, *Phys. Chem. Chem. Phys.* **15**, 14961 (2013).
- [22] D. Chen, J. H. Porada, J. B. Hooper, A. Klittnick, Y. Shen, M. R. Tuchband, E. Korblova, D. Bedrov, D. M. Walba, M. A. Glaser, J. E. MacLennan, and N. A. Clark, *Proc. Natl. Acad. Sci. USA* **110**, 15931 (2013).
- [23] V. P. Panov, R. Balachandran, M. Nagaraj, J. K. Vij, M. G. Tamba, and A. Kohlmeier, *Appl. Phys. Lett.* **99**, 261903 (2011).
- [24] V. P. Panov, R. Balachandran, J. K. Vij, M. G. Tamba, A. Kohlmeier, and G. H. Mehl, *Appl. Phys. Lett.* **101**, 234106 (2012).
- [25] C. Meyer, G. R. Luckhurst, and I. Dozov, *Phys. Rev. Lett.* **111**, 067801 (2013).
- [26] C. Greco, G. R. Luckhurst, and A. Ferrarini, *Soft Matter* **10**, 9318 (2014).
- [27] A. G. Hoffmann, A. Vanakaras, A. Kohlmeier, G. H. Mehl, and D. J. Photinos, *Soft Matter* **11**, 850 (2015).
- [28] M. Cifelli, S. V. Dvinskikh, and G. R. Luckhurst, presented at 25th International Liquid Crystal Conference, ILCC 2014, Dublin (unpublished).
- [29] M. B. Sied, J. Salud, D. O. López, M. Barrio, and J. Ll. Tamarit, *Phys. Chem. Chem. Phys.* **4**, 2587 (2002).
- [30] M. A. Anisimov, *Critical Phenomena in Liquids and Liquid Crystals* (Gordon and Breach Science Publishers, Amsterdam, 1991), and references therein.
- [31] P. H. Keyes and J. R. Shane, *Phys. Rev. Lett.* **42**, 722 (1979).
- [32] P. Cusmin, M. R. de la Fuente, J. Salud, M. A. Pérez-Jubindo, S. Diez-Berart, and D. O. López, *J. Phys. Chem. B* **111**, 8974 (2007).
- [33] J. Salud, P. Cusmin, M. R. de la Fuente, M. A. Pérez-Jubindo, D. O. López, and S. Diez-Berart, *J. Phys. Chem. B* **113**, 15967 (2009).
- [34] G. S. Iannacchione and D. Finotello, *Phys. Rev. E* **50**, 4780 (1994).
- [35] S. Diez, D. O. López, M. R. de la Fuente, M. A. Pérez-Jubindo, J. Salud, and J. Ll. Tamarit, *J. Phys. Chem. B* **109**, 23209 (2005).
- [36] E. G. Virga, *Phys. Rev. E* **89**, 052502 (2014).
- [37] C. Meyer, G. R. Luckhurst, and I. Dozov, *J. Mater. Chem. C* **3**, 318 (2015).
- [38] E. I. Kats and V. V. Levedev, *JETP Lett.* **100**, 110 (2014).
- [39] A. Ferrarini, G. R. Luckhurst, P. L. Nordio, and S. J. Roskilly, *Chem. Phys. Lett.* **214**, 409 (1993).
- [40] A. Ferrarini, G. R. Luckhurst, P. L. Nordio, and S. J. Roskilly, *Liq. Cryst.* **21**, 373 (1996).
- [41] M. Stocchero, A. Ferrarini, G. J. Moro, D. A. Dunmur, and G. R. Luckhurst, *J. Chem. Phys.* **121**, 8079 (2004).
- [42] D. A. Dunmur, G. R. Luckhurst, M. R. de la Fuente, S. Diez, and M. A. Pérez-Jubindo, *J. Chem. Phys.* **115**, 8681 (2001).
- [43] N. Sebastián, M. R. de la Fuente, D. O. López, M. A. Pérez-Jubindo, J. Salud, and M. B. Ros, *J. Phys. Chem. B* **117**, 14486 (2013).
- [44] N. Sebastián, M. R. de la Fuente, D. O. López, M. A. Pérez-Jubindo, J. Salud, S. Diez-Berart, and M. B. Ros, *J. Phys. Chem. B* **115**, 9766 (2011).
- [45] J. P. Jokisaari, G. R. Luckhurst, B. A. Timimi, J. Zhu, and H. Zimmermann, *Liq. Cryst.* **42**, 708 (2015).
- [46] C. J. Yun, M. R. Vengatesan, J. K. Vij, and J. K. Song, *Appl. Phys. Lett.* **106**, 173102 (2015).
- [47] S. W. Morris, P. Palfy-Muhoray, and D. A. Balzarini, *Mol. Cryst. Liq. Cryst.* **139**, 263 (1986).
- [48] M. G. Clark, E. P. Raynes, R. A. Smith, and R. J. A. Tough, *J. Phys. D: Appl. Phys.* **13**, 2151 (1980).
- [49] N. Sebastián, B. Robles-Hernández, D. O. López, M. R. de la Fuente, S. Diez-Berart, J. Salud, D. Dunmur, and G. R. Luckhurst, presented at 25th International Liquid Crystal Conference, ILCC 2014, Dublin (unpublished).
- [50] B. Kundu, R. Pratibha, and N. V. Madhusudana, *Phys. Rev. Lett.* **99**, 247802 (2007).
- [51] P. Sathyanarayana, V. S. R. Jampani, M. Skarabot, I. Musevic, K. V. Le, H. Takezoe, and S. Dhara, *Phys. Rev. E* **85**, 011702 (2012).
- [52] C. T. Imrie and G. R. Luckhurst, in *Handbook of Liquid Crystals*, edited by J. W. Goodby, P. J. Collings, T. Kato, C. Tschierske, H. F. Gleeson, and P. Raynes (Wiley-VCH, Weinheim, 2014), Vol. 7, Part II.
- [53] G. R. Luckhurst, *Macromol. Symp.* **96**, 1 (1995).
- [54] A. Kloczkowski, G. R. Luckhurst, and R. W. Phippen, *Liq. Cryst.* **3**, 185 (1998).
- [55] A. Emerson, G. R. Luckhurst, and R. W. Phippen, *Liq. Cryst.* **10**, 1 (1991).

